Annu. Rev. Mater. Sci. 2000. 30:387–429

MAGNETOCALORIC MATERIALS

K. A. Gschneidner, Jr. and V. K. Pecharsky
Ames Laboratory and Department of Materials Science and Engineering, Iowa State University, Ames, Iowa 50011-3020; e-mail: cagey@ameslab.gov

Key Words magnetocaloric effect, mixed lanthanide materials, 3*d*-materials amorphous alloys, manganites

■ **Abstract** In the last decade of the twentieth century there has been a significant increase in research on a more than 100-year old phenomenon—the magnetocaloric effect (MCE). As a result, many new materials with large MCEs (and many with lesser values) have been discovered, and a much better understanding of this magneto-thermal property has resulted. In this review we briefly discuss the principles of magnetic cooling (and heating); the measurement of the magnetocaloric properties by direct and indirect techniques; the special problems that can arise; and the MCE properties of the 4*f* lanthanide metals, their intra-lanthanide alloys and their compounds [including the giant MCE $Gd_5(Si_xGe_{1-x})_4$ phases]; the 3*d* transition metals, their alloys and compounds; and mixed lanthanide-3*d* transition metal materials (including the La manganites).

INTRODUCTION

Commercial and residential refrigeration is a mature, relatively low capital cost but a high-energy demand industry. Even the newest most efficient units operate well below the maximum theoretical (Carnot) efficiency, and few, if any, further improvements may be possible with the existing vapor-cycle technology. Magnetic refrigeration (MR), however, is rapidly becoming competitive with conventional gas compression technology because it offers considerable operating cost savings by eliminating the most inefficient part of the refrigerator—the compressor. In addition to its energy savings potential, MR is an environmentally sound alternative to vapor-cycle refrigerators and air conditioners. Most modern refrigeration systems and air conditioners still use ozone-depleting or global-warming volatile liquid refrigerants. Magnetic refrigerators use a solid refrigerant(s) and common heat transfer fluids (e.g. water, water-alcohol solution, air, or helium gas) with no ozone-depleting and/or global-warming effects.

Magnetic refrigeration is based on the magnetocaloric effect (MCE). The MCE, or adiabatic temperature change (ΔT_{ad}), which is detected as the heating or the cooling of magnetic materials due to a varying magnetic field, was originally discovered in iron by Warburg (1). The thermodynamics of the MCE was understood

by Debye (2) and by Giauque (3), both of whom independently suggested that it could be used to reach low temperatures in a process known as adiabatic demagnetization. Soon after this discovery, an operating adiabatic demagnetization refrigerator was constructed and utilized by Giauque & McDougal (4) to reach 0.53, 0.34, and 0.25 K starting at 3.4, 2.0, and 1.5 K, respectively, using a magnetic field of 0.8 T and 61 g of $Gd_2(SO_4)_3{\cdot}8H_2O$ as the magnetic refrigerant. The MCE is intrinsic to any magnetic material. In the case of a ferromagnet near its magnetic ordering temperature, the adiabatic application of a magnetic field reduces the magnetic entropy of a solid and, in turn, it is heated via the increase of its lattice entropy to maintain the entropy of a closed system at a constant value. In a reversible process, a ferromagnet is cooled as the magnetic entropy increases, and the lattice entropy decreases upon adiabatic removal of the magnetic field. The warming and the cooling of a magnetic material in response to a changing magnetic field is similar to the warming and the cooling of a gaseous medium in response to an adiabatic compression and expansion. Therefore, MR operates by magnetizing/demagnetizing the magnetic material. Since the refrigerant is a solid (usually in a form of spheres or thin sheets), the heat transfer is provided by a fluid (e.g. water, water with antifreeze, or an inert gass, depending on the operating temperature).

We discuss the magnetocaloric properties of selected classes of magnetic materials, describing their potential as magnetic refrigerants for a variety of temperature ranges. Two aspects of a successful magnetic refrigerator, not considered here, are (*a*) the performance of the magnetic field sources, which substitute for the compressor and evaporator, and (*b*) the engineering of the magnetic refrigerator, which includes the design of the refrigeration cycle, the organization of the heat transfer fluid flow and the heat exchange. Instead, we direct the interested reader to several technical papers (4–22).

The MCE ΔS_M (isothermal magnetic entropy change) values are reported in various units in the literature. In this review the published data have been converted to mJ/cm^3 K units for two reasons: one, for uniformity so that various MCE values reported for the same materials (or for other materials) can be readily compared with one another; two, because some of the materials may be actually used in MRs, the most meaningful parameter for the engineer designing the MR with a limited high-magnetic field volume is the cooling power per unit volume.

PRINCIPLES OF MAGNETIC COOLING AND HEATING

When magnetic material is subject to a magnetic field changing by $\Delta H = H_F - H_I$ at constant pressure (the subscripts F and I indicate the final and the initial magnetic field strength, respectively), two different processes may occur in a magnetic material. The first is the isothermal process that occurs when the magnetic field is altered but the material remains connected to the surroundings (heat sink/heat reservoir) and, therefore, remains at constant temperature. The entropy of a magnetic solid

is then changed by

$$\Delta S_M(T)_{\Delta H} = \left(S(T)_{H_F} - S(T)_{H_I}\right)_T \quad 1.$$

and $\Delta S_M(T)_{\Delta H}$ is conventionally called magnetic entropy change. The magnetic entropy change of a solid directly characterizes the cooling capacity, q, of the magnetic material

$$q = -\int_{T_1}^{T_2} \Delta S_M(T)_{\Delta H}\, dT, \quad 2.$$

which indicates how much heat can be transferred from the cold end (at T_1) to the hot end (at T_2) of the refrigerator in one ideal thermodynamic cycle. The second is an adiabatic process that occurs when the magnetic field is modified but the material is isolated from the surroundings and, therefore, the total entropy of a solid remains constant. The temperature of a magnetic material is then changed by

$$\Delta T_{ad}(T)_{\Delta H} = \left(T(S)_{H_F} - T(S)_{H_I}\right)_S \quad 3.$$

and $\Delta T_{\mathrm{ad}}(T)_{\Delta H}$ is conventionally called adiabatic temperature change. The adiabatic temperature change indirectly characterizes both the cooling capacity and the temperature difference between the cold and the hot ends of the refrigerator (generally a larger ΔT_{ad} corresponds to a larger cooling capacity of the material and to a larger temperature span of the refrigerator). It should be noted that the difference between the hot end and the cold end temperatures of a magnetic refrigerator greatly exceeds that of the maximum magnetocaloric effect in a properly designed active magnetic regenerator cycle (8–10, 21).

If both the magnetization and entropy are continuous functions of the temperature and magnetic field, then the infinitesimal isobaric-isothermal magnetic entropy change can be related to the magnetization (M), the magnetic field strength (H), and the absolute temperature (T) using one of the Maxwell relations (23)

$$\left(\frac{\partial S_M(T, H)}{\partial H}\right)_T = \left(\frac{\partial M(T, H)}{\partial T}\right)_H, \quad 4.$$

which after integration yields

$$\Delta S_M(T)_{\Delta H} = \int_{H_I}^{H_F} dS_M(T, H)_T = \int_{H_I}^{H_F} \left(\frac{\partial M(T, H)}{\partial T}\right)_H dH. \quad 5.$$

By combining Equation 4 and the following Equation 6

$$\left(\frac{\partial S(T, H)}{\partial T}\right)_H = \left(\frac{C(T, H)}{T}\right)_H \quad 6.$$

and 7

$$TdS = T\left(\frac{\partial S(T, H)}{\partial T}\right)_H dT + T\left(\frac{\partial S(T, H)}{\partial H}\right)_T dH \quad 7.$$

it is easy to show (23) that the infinitesimal adiabatic ($TdS = 0$) temperature rise for the reversible adiabatic-isobaric process is

$$dT(T, H) = -\left(\frac{T}{C(T, H)}\right)_H \left(\frac{\partial M(T, H)}{\partial T}\right)_H dH, \qquad 8.$$

where $C(T, H)$ is the temperature and magnetic field-dependent heat capacity at constant pressure. $\Delta T_{ad}(T)_{\Delta H}$ is obtained by integrating Equation 8 as

$$\Delta T_{ad}(T)_{\Delta H} = \int_{H_I}^{H_F} dT(T, H) = -\int_{H_I}^{H_F} \left(\frac{T}{C(T, H)}\right)_H \left(\frac{\partial M(T, H)}{\partial T}\right)_H dH. \qquad 9.$$

Both $\Delta S_M(T)_{\Delta H}$ and $\Delta T_{\text{ad}}(T)_{\Delta H}$ depend on temperature and ΔH (Equations 5 and 9, respectively) and are usually studied and reported as functions of temperature for a given ΔH, or as functions of ΔH for a given temperature. The behavior of both characteristics of the magnetocaloric effect, i.e. $\Delta S_M(T)_{\Delta H}$ and $\Delta T_{\text{ad}}(T)_{\Delta H}$, is material dependent, cannot be easily predicted from the first principles, and therefore, must be experimentally measured. The heavy lanthanide metals and their compounds were always considered the best potential magnetocaloric materials because they have the largest magnetic moments (and, therefore, the most favorable bulk magnetizattion and potentially a large $|\partial M/\partial T|$; see Equations 4 and 9) and the largest available magnetic entropy (Figure 1). In this review we are concerned with

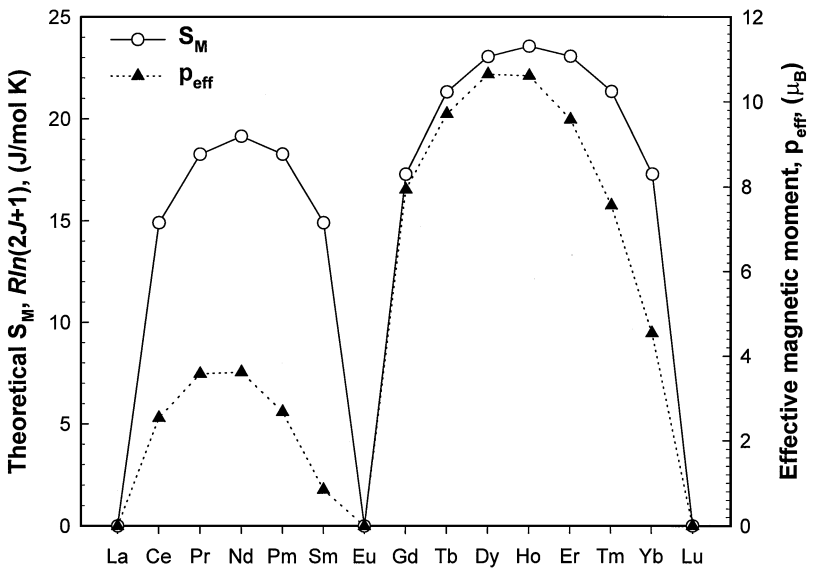

Figure 1 Theoretical molar magnetic entropy, S_M, (*left scale*) and effective magnetic moment of free R^{3+} ions, p_{eff}, (*right scale*) of the lanthanide elements.

only the magnetocaloric properties of materials in the temperature range away from absolute zero, which can be used for continuous cooling, e.g. for air conditioning, household and commercial refrigeration/freezing, and gas liquefaction.

Conventional Behavior

It is easy to see that both $\Delta S_M(T)_{\Delta H}$ and $\Delta T_{\rm ad}(T)_{\Delta H}$ are proportional to the derivative of the magnetization with respect to temperature at constant magnetic field (Equations 5 and 9). $\Delta T_{\rm ad}(T)_{\Delta H}$ is also proportional to the absolute temperature and inversely proportional to the heat capacity at constant magnetic field. Therefore, it is expected that any material should have the largest $\Delta S_M(T)_{\Delta H}$ and $\Delta T_{\rm ad}(T)_{\Delta H}$ when its magnetization is changing rapidly with temperature, i.e. in the vicinity of a spontaneous magnetic-ordering temperature. The MCE gradually decreases both below (magnetization is nearly saturated and is weakly dependent on the temperature in an ordered state) and above (magnetization shows only a paramagnetic response) the magnetic-ordering temperature (24).

Therefore, conventional ferromagnets typically display a "caret-like" $\Delta S_M(T)_{\Delta H}$ and $\Delta T_{\rm ad}(T)_{\Delta H}$. This is shown in Figure 2 for pure single crystalline Gd (25), which orders ferromagnetically at 294 K. Hence, numerical characterization of magnetocaloric materials with conventional MCE behavior is possible by specifying the temperature of the MCE peak, its magnitude (ΔS_M or ΔT_{ad}), and its full width at half maximum (δT_{FWHM}). In the case of magnetic entropy change, a product of the ΔS_M maximum and full width at half maximum ($\delta T_{FWHM} = T_2 - T_1$; see Figure 2*a*) yields close to 4/3 times the cooling capacity (Equation 2) in the temperature range from T_1 to T_2. This is easy to prove using a simple geometrical approach if one assumes that the caret-like shape of the MCE peak can be approximated by a triangle. For example, the integration of the data from Figure 2*a* for magnetic field change from 0 to 2 *T* using Equation 2 yields the cooling capacity, *q*, of ~1.37 J/cm^3 for Gd between $T_1 = 276$ and $T_2 = 315$ K, while the value calculated as 3/4 of $-\Delta S_M(max) \times \delta T_{FWHM}$ is ~1.39 J/cm^3, i.e. the difference is less than 2%. Therefore, we will call the product

$$RCP(S) = -\Delta S_M(\max) \times \delta T_{FWHM}, \qquad 10.$$

the relative cooling power (RCP) based on the magnetic entropy change. Similarly, the MCE measured as the adiabatic temperature change, ΔT_{ad}, can be numerically characterized by the MCE maximum and the δT_{FWHM} of the MCE peak (see Figure 2*b*). The product

$$RCP(T) = -\Delta T_{ad}(\max) \times \delta T_{FWHM} \qquad 11.$$

will be called a relative cooling power based on the adiabatic temperature change. It has K^2 dimension and no physical meaning, but may be useful for numerical comparison of different magnetocaloric materials, especially when no ΔS_M values are available. A large $RCP(T)$ for the same ΔH generally indicates a better magnetocaloric material. Both peak values [$\Delta S_M(\Delta H)_T$ and/or $\Delta T_{\rm ad}(\Delta H)_T$] and

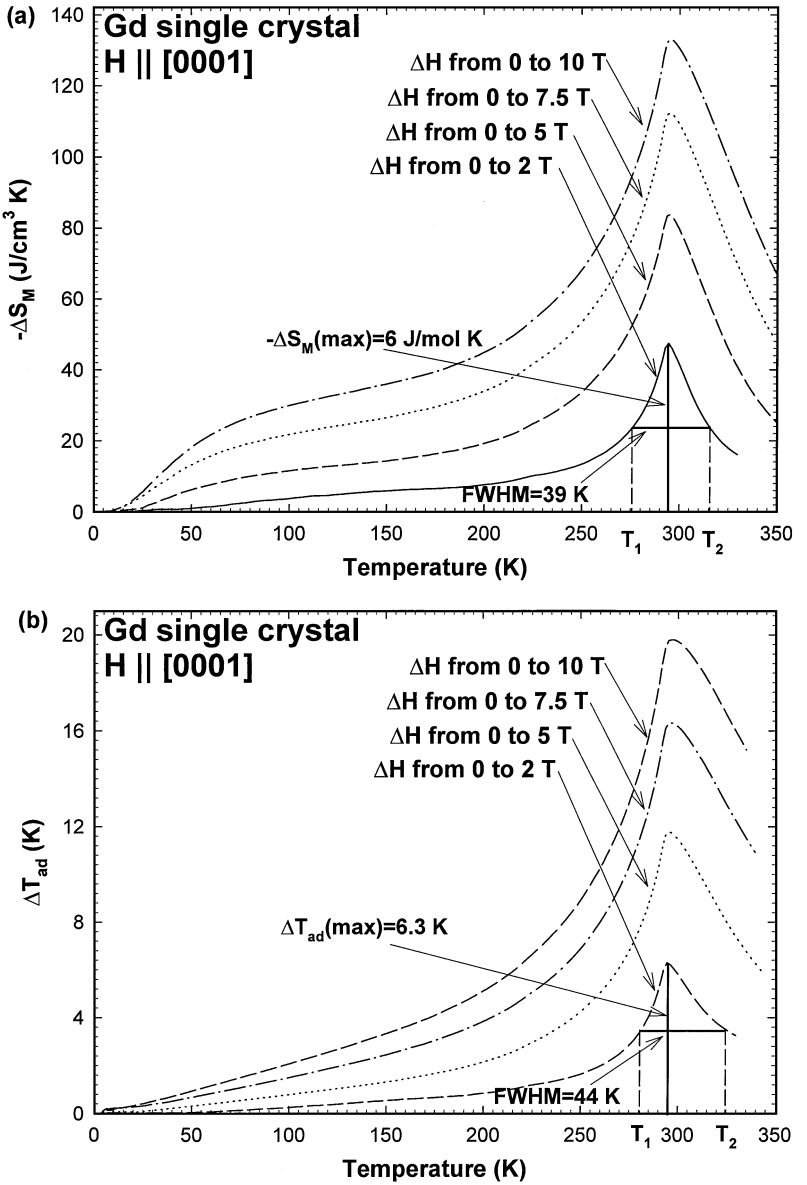

Figure 2 An example of the conventional caret-like behavior of (*a*) $\Delta S_M(T)_{\Delta H}$ and (*b*) $\Delta T_{ad}(T)_{\Delta H}$ in single crystal-Gd as calculated from the heat capacity data (25). The data for ΔH from 0 to 2T in (*a*) and (*b*) also show the peak value and the full width at half maximum (FWHM) along with corresponding T_1 and T_2 used to numerically characterize the relative cooling power [*RCP*(*S*) and *RCP*(*T*), respectively] of the material.

δT_{FWHM} usually increase with the increasing ΔH. The one-to-one correspondence of ΔS_M and ΔT_{ad}, and of $RCP(S)$ and $RCP(T)$ are shown in Figures 3*a* and *b*, respectively, for a series of pseudo-binary $DyAl_2$-$ErAl_2$ alloys.

Conventional magnetocaloric effect behavior can be also characterized by reporting the values of $\Delta S_M(\Delta H)_T$ and/or $\Delta T_{ad}(\Delta H)_T$ as a function of ΔH for a given temperature, which usually is taken at the MCE maximum. This is shown for Gd in Figure 4, where the data reported by various authors (7, 25–34), measured on different samples of Gd using different experimental techniques (see below), are combined. It is easy to see that the magnetocaloric effect continues to rise with ΔH, but its rate of change [or the specific magnetocaloric effect, $d\Delta T_{\rm ad}(\Delta H)_T/d\Delta H$] decreases. The ideal linear behavior of the latter seen in Figure 4 (dotted line) is an artifact because the MCE data were fitted to a second order polynomial (solid line drawn through the data points in Figure 4), excluding the four most likely erroneous data points reported in References 32–34, which after differentiation must yield a straight line. Nevertheless, Figure 4 provides a good illustration of a universal behavior observed in all ferromagnetic magnetocaloric materials, i.e. that the specific magnetocaloric effect is the highest for the lowest ΔH, gradually decreasing as ΔH increases, thus indicating that MCE has a tendency to saturate in sufficiently high magnetic fields.

Anomalous Magnetocaloric Effect

The anomalous behavior of the magnetocaloric effect is closely related to the anomalous changes in the magnetic structure of solids that cause an unusual behavior of $\partial M/\partial T$ and $C(T, H)$, which carries over to both $\Delta S_M(T)_{\Delta H}$ and $\Delta T_{\rm ad}(T)_{\Delta H}$ (see Equations 4, 5, 8, and 9). One of the most commonly observed MCE anomalies occurs when a material undergoes two or more successive magnetic orderings in close proximity to one another. Then, instead of a conventional caret-like shape, a "skewed caret" sometimes approaching a flat and almost constant (i.e. a "table-like") MCE $(T)_{\Delta H}$ can be observed. One such example is given in Figure 5 showing the magnetocaloric effect in $(Gd_{0.6}Er_{0.4})AlNi$ (35). The behavior of $\Delta S_M(T)_{\Delta H}$ (Figure 5*a*) is a skewed caret, whereas the $\Delta T_{ad}(T)_{\Delta H}$ (Figure 5*b*) is almost constant between 16 and 36 K. An anomalous MCE behavior may be observed, not only in materials with multiple magnetic orderings, but also in materials with low lying crystalline electric field levels, as reported for $(Dy_{0.5}Er_{0.5})Al_2$ (36, 37) and also shown in Figure 5. Here the lower-temperature rounded peak of both the magnetic entropy and the adiabatic temperature change is associated with the suppression of the Schottky anomaly by increasing magnetic field; the well defined upper caret–shaped peak is due to a ferromagnetic ordering in the material.

Generally, the more complicated the magnetic structure of the material the more complicated the anomalous behavior of the MCE. For instance, upon cooling in zero magnetic field pure Dy orders antiferromagnetically at ~180 K with a helical

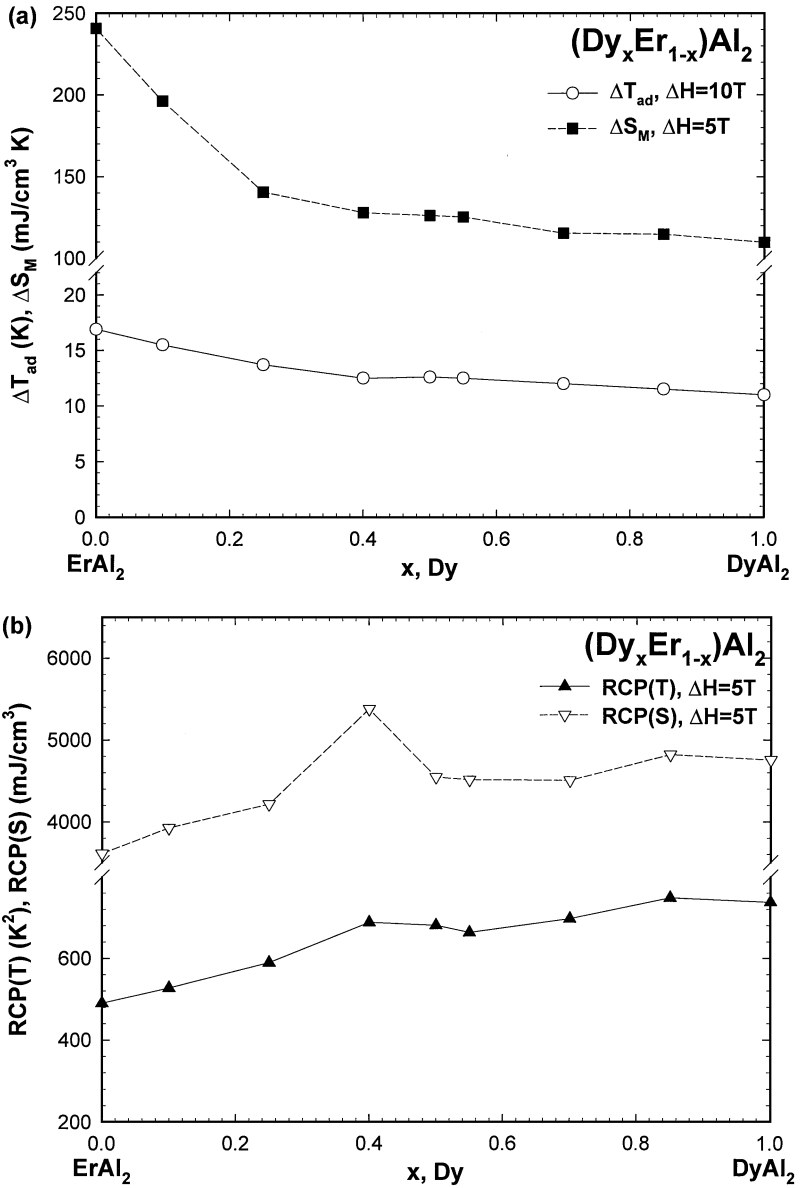

Figure 3 (*a*) The magnetocaloric effect ΔS_M and ΔT_{ad} (*b*) and the relative cooling powers *RCP*(*S*) and *RCP*(*T*) as a function of the Dy content for the $(Dy_xEr_{1-x})Al_2$ alloys.

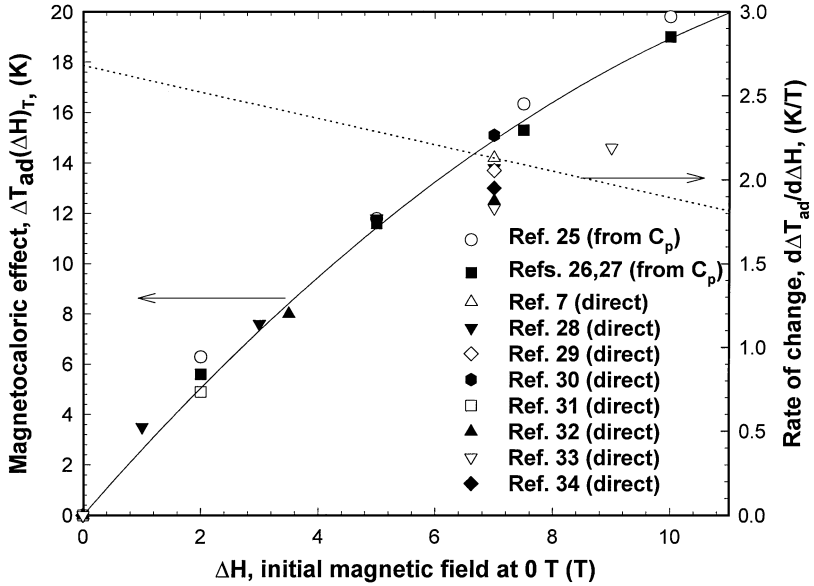

Figure 4 The maximum magnetocaloric effect in Gd observed at the Curie temperature of the material as a function of magnetic field change (solid line and data points; *left scale*) and the MCE rate of change (dotted line; *right scale*).

magnetic structure, and then a transition from a helical antiferromagnet to a ferromagnet occurs at ∼90 K (38). Accordingly when the magnetic field is low, the MCE shows a sharp step-like increase at ∼90 K due to a first order ferromagnetic-antiferromagnetic (and simultaneous orthorhombic-hexagonal close-packed structural) transition, and then goes through a minimum immediately followed by a weak maximum at ∼180 K for $\Delta H = 1$ T (as shown in Figure 6) (24). The minimum exists because the application of magnetic field to an antiferromagnet increases the magnetic entropy inverting the sign of MCE (in a ferromagnet the increasing field decreases magnetic entropy). When the magnetic field increases to 2 T it becomes strong enough to quench the first order ferromagnetic-antiferromagnetic phase transition thereby inducing non-collinear magnetic structure, which yields a broad MCE maximum at ∼127 K. Because a 2 T magnetic field is not strong enough to destroy this non-collinear structure, the slightly negative ΔT_{ad} is still observed at ∼174 K and is followed by a caret-type peak at ∼181 K (Figure 6). Upon increasing magnetic field to 5 T, it becomes strong enough to suppress all magnetic structures except the ferromagnetic phase, and the MCE for $\Delta H = 5$ T has a single skewed caret-type peak at ∼181 K.

Most magnetic materials on cooling undergo a second order phase transition from a paramagnet to a ferromagnet with the conventional MCE behavior

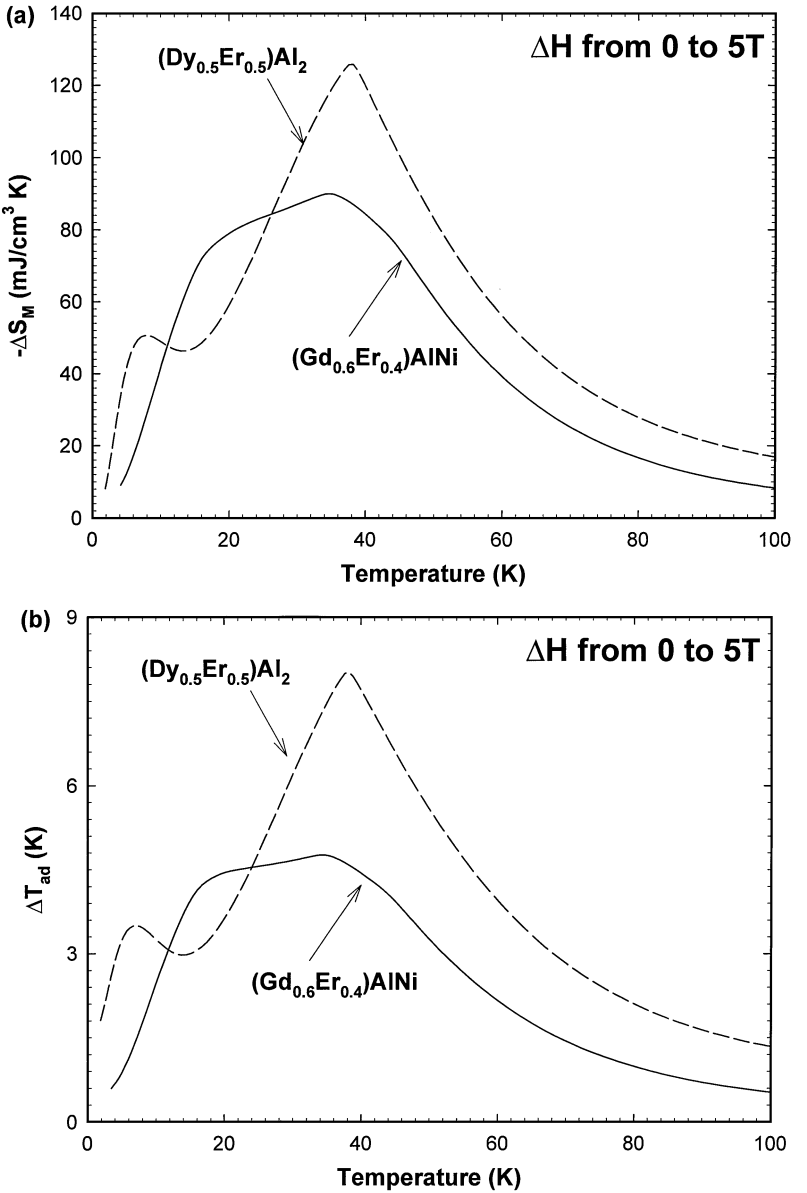

Figure 5 Examples of the skewed caret (table-like) and multiple peak behavior of (*a*) $\Delta S_M(T)_{\Delta H}$ and (*b*) $\Delta T_{ad}(T)_{\Delta H}$ in $(Gd_{0.6}Er_{0.4})AlNi$ (35) compared with the normal caret-like behavior (at ~40 K) $(Dy_{0.5}Er_{0.5})Al_2$ (36, 37).

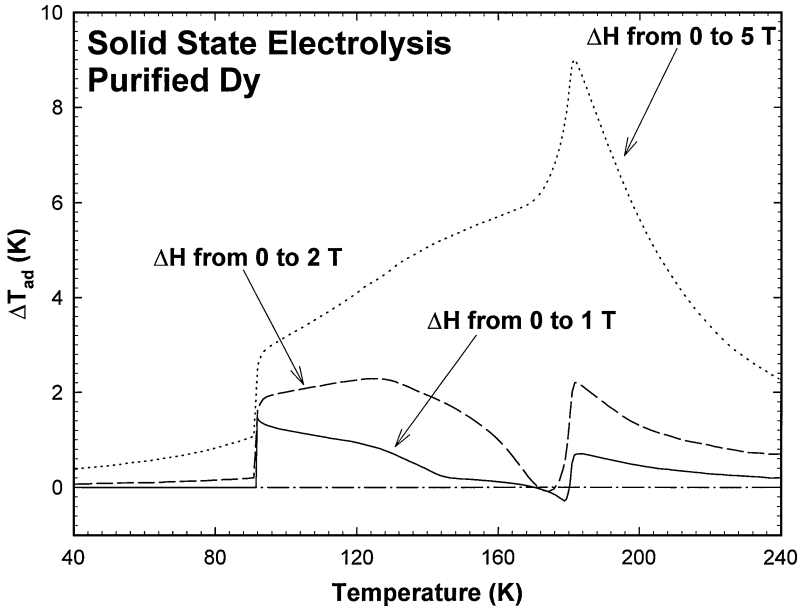

Figure 6 The magnetocaloric effect in ultra-pure Dy calculated from the heat capacity data (24).

(Figure 2), or from a paramagnet to an antiferromagnet with a skewed caret MCE if the magnetic field is high enough to destroy the antiferromagnetism, thus converting it to a ferromagnetic structure (Figure 6). A few materials, however, form the ferromagnetically ordered phase from the paramagnetic state through a first order magnetic phase transition. The most interesting example is found in the $Gd_5(Si_xGe_{1-x})_4$ alloys where $0 \leq x \leq 0.5$ (39–42). Here, since the phase transition is of the first order, the $|\partial M/\partial T|$ is larger than usual (but not infinite and undefined as could happen if the transition occurs infinitely fast at constant temperature, pressure and magnetic field) and, therefore, the magnetocaloric effect is also large (see Equations 4, 5, 8, and 9). In Figure 7 it is easy to see that increasing the magnetic field beyond 3 T hardly increases the maximum magnetocaloric effect, but continues to increase considerably the δT_{FWHM}, which shifts the upper temperature limit of the MCE toward higher temperatures and, therefore, continues to increase the cooling capacity of the material. The lower temperature MCE limit (Figure 7) remains practically independent of the ΔH because it is determined by the temperature where the transition occurs at the lowest magnetic field (in this case 0 T). We call this type of anomalous behavior a sky-scraper magnetocaloric effect. Other than the $Gd_5(Si_xGe_{1-x})$ alloys there is only one other material, FeRh (43–45), that exhibits the giant magnetocaloric effect near room temperature. However, the MCE in FeRh is irreversible.

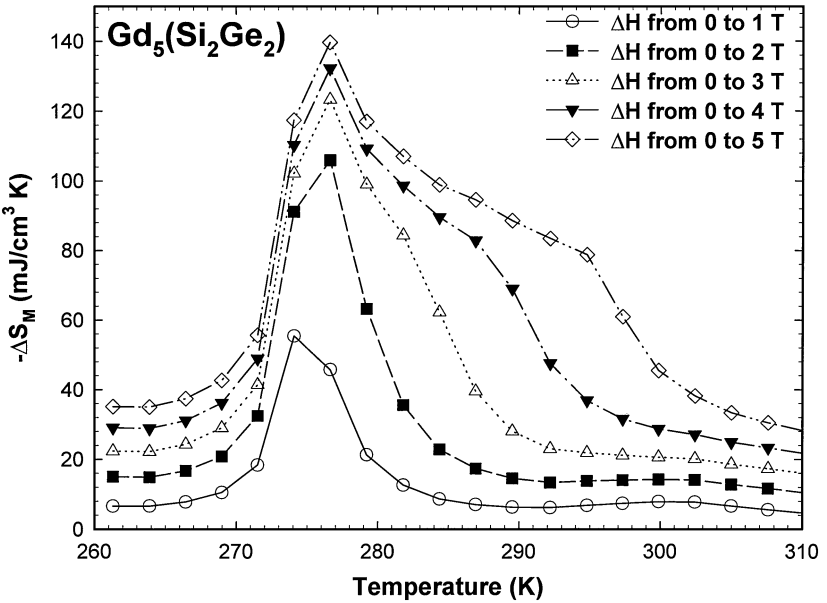

Figure 7 The magnetocaloric effect in $Gd_5(Si_2Ge_2)$ calculated from the magnetization data (39).

MEASUREMENTS OF THE MAGNETOCALORIC EFFECT

The magnetocaloric effect can be measured (direct techniques) or calculated (indirect techniques) from the measured magnetization or heat capacity, both as a function of temperature and magnetic field. The direct and indirect techniques have certain advantages and disadvantages.

The direct techniques provide only one measure of the magnetocaloric effect, the adiabatic temperature change. Since the temperatures are measured directly, no further processing of data except subtraction of the two numbers is involved. However, direct measurements are usually time-consuming and are difficult to perform at small temperature step intervals. A comprehensive analysis of the errors is hardly possible, and the error estimate is usually based on comparison of the measured data using any standard material. If the direct measurement apparatus is not properly calibrated, or if the material is not properly isolated, large experimental errors become inevitable, especially if the ΔT_{ad} values are large (i.e. >10 K). For example, see Figure 4, where there are three low points at 7 T and one low point at 9 T. Furthermore, the magnetic field by definition must be changed as quickly as possible. This may cause problems if the studied materials are poor conductors (this is almost always the case because magnetic materials near their ordering

temperature have low thermal conductivities), or when phase transitions involved exhibit non-infinite kinetics.

Unlike the direct MCE measurements, which yield only the adiabatic temperature change, the indirect experiments allow the calculation of both $\Delta T_{ad}(T)_{\Delta H}$ and $\Delta S_M(T)_{\Delta H}$ from experimental heat capacity data, or $\Delta S_M(T)_{\Delta H}$ alone from experimental magnetization data. Indirect techniques provide results at practically any temperature interval. However, considerable processing of experimental data is involved before the MCE is calculated. Also on the positive side, indirect techniques allow comprehensive error analysis as long as the accuracy of experimental data (heat capacity or magnetization) is known (see below).

Direct Measurements

Direct MCE measuring techniques always involve measurements of the sample temperatures (T_I and T_F) in magnetic fields H_I and H_F, where subscripts I and F designate initial and final magnetic field, respectively. $\Delta T_{ad}(T)_{\Delta H}$ is then determined as the difference

$$\Delta T_{ad}(T_I)_{\Delta H} = T_F - T_I \qquad 12.$$

for a given T_I and $\Delta H = H_F - H_I$. The MCE is usually measured during field increase and decrease, and the results are reported as the function of initial temperature for a given ΔH.

Direct MCE measurements can be carried out using contact (i.e. when the temperature sensor is in direct thermal contact with the sample) and non-contact techniques (i.e. when the sample temperature is measured without the sensor being directly connected to the sample) (30, 33, 46–52). Since during the direct MCE measurements a rapid change of the magnetic field is generally required, the measurements can be carried out on immobilized samples when the magnetic field change is provided either by charging/discharging the magnet, or by moving the sample in and out of a uniform magnetic field volume. Using immobilized samples and pulse magnetic fields, direct MCE measurements in magnetic fields from 1 to 40 T have been reported. The use of electromagnets usually limits the magnetic field strength up to a maximum of about 2 T. Experimental apparati, where the sample or the magnet is moved to provide the varying magnetic field environment usually employ superconducting or permanent magnets, which limit the magnetic field range to 0 to 10 T, and 0.1 to 2.0 T, respectively. The accuracy of the direct experimental techniques depends on the errors in thermometry, errors in field setting, the quality of thermal isolation of the sample (this becomes a critical source of error when the MCE is large and thus disrupts the adiabatic conditions), and the quality of the compensation circuitry to eliminate the effect of the changing magnetic field on the temperature sensor. Considering all these effects the accuracy is claimed to be in the 5 to 10% range (30, 33, 46–52). The errors, however, may be considerably larger, particularly if one of the issues

(see above) affecting the accuracy is not resolved properly. To illustrate the possibility of the directly measured magnetocaloric effect error exceeding the usual 5 to 10% range, one simply needs to examine Figure 4, where some data deviate from each other by as much as 20 to 25%.

Indirect Measurements from Magnetization

Magnetization measured experimentally as a function of temperature and magnetic field provides $\Delta S_M(T)_{\Delta H}$ after numerical integration of Equation 5 and is a useful technique for the rapid screening of prospective magnetic refrigerant materials (53). Numerical integration of Equation 5 is straightforward, and the experimental errors in the $\Delta S_M(T)_{\Delta H}$ depend on the errors in temperature, magnetic moment, and magnetic field. Because numerical integration is involved, and because the exact differentials (dM, dT, and dH) are substituted, respectively, by the measured ΔM, ΔT, and ΔH, the typical accuracy of $\Delta S_M(T)_{\Delta H}$ from magnetization measurements without the proper error analysis was reported to be about $\pm 7.5\%$ error in the values of $\Delta S_M(T)_{\Delta H}$ if magnetization data are measured with 0.5% accuracy (53). When the errors are analyzed comprehensively, it was shown (54) that they are given as

$$\sigma|\Delta S_M(T_{av})_{\Delta H}| = \frac{1}{2|\delta T|}\left\{|\delta H| \times \left(\sigma M_1 + 2\sum_{k=2}^{n-1}\sigma M_k + \sigma M_n\right) + \left(|\delta M_1|\sigma H_1 + 2\sum_{k=2}^{n-1}(|\delta M_k|\sigma H_k) + |\delta M_n|\sigma H_n\right) + 2|\Delta S_M(T_{av})_{\Delta H}| \times (\sigma T_2 + \sigma T_1)\right\}, \quad 13.$$

where σ is the experimental error in the corresponding parameter, δ corresponds to the step in actual experimental data, T_{av} is $(T_1 + T_2)/2$ for the two magnetization isotherms measured at T_1 and T_2, and n is the total number of magnetization data points measured for each isotherm. Consequently, the errors in the $\Delta S_M(T)_{\Delta H}$ calculated from magnetization data can be as high as 20 to 30% (54).

Indirect Measurements from Heat Capacity

The heat capacity measured at constant pressure as a function of temperature in constant magnetic fields, $C(T)_H$, provides the most complete characterization of solid magnetic materials with respect to their magnetocaloric effect, since the total entropy of a magnetic solid can be calculated from the heat capacity as

$$S(T)_{H_I} = \int_0^T \frac{C(T)_{H_I}}{T}\,dT + S_{0,H_I}, \text{ and } S(T)_{H_F} = \int_0^T \frac{C(T)_{H_F}}{T}\,dT + S_{0,H_F}, \quad 14.$$

where S_{0,H_I} and S_{0,H_F} are the zero temperature entropies. In a condensed system these are the same (i.e. $S_{0,H_I} = S_{0,H_F}$), and therefore, can be neglected.

Once the total entropy functions, $S(T)_{H_I}$ and $S(T)_{H_F}$, are established, the calculation of both $\Delta T_{ad}(T)_{\Delta H}$ and $\Delta S_M(T)_{\Delta H}$ becomes straightforward. The $\Delta S_M(T)_{\Delta H}$ is calculated as the isothermal difference (Equation 15) and the $\Delta T_{ad}(T)_{\Delta H}$ is calculated as the isentropic difference (Equation 16) between the $S(T)_{H_I}$ and $S(T)_{H_F}$ functions.

$$\Delta S_M(T)_{\Delta H} = \left(S(T)_{H_F} - S(T)_{H_I}\right)_T \qquad 15.$$

$$\Delta T_{ad}(T)_{\Delta H} \cong \left(T(S)_{H_F} - T(S)_{H_I}\right)_S \qquad 16.$$

Based on Equation 15, the error in $\Delta S_M(T)_{\Delta H}$ resulting from accumulation of random experimental errors in the total entropy is given (54) as

$$\sigma|\Delta S_M(T)_{\Delta H}| = \left(\sigma S(T)_{H_I} + \sigma S(T)_{H_F}\right)_T, \qquad 17.$$

and the error in $\Delta T_{ad}(T)_{\Delta H}$ is also easily derived from Equation 16 (54) as

$$\sigma|\Delta T_{ad}(T)_{\Delta H}| = \left[\sigma S(T)_{H_F}\frac{T}{C(T)_{H_F}} + \sigma S(T)_{H_I}\frac{T}{C(T)_{H_I}}\right]_S. \qquad 18.$$

The errors in the total entropy, $\sigma S(T)_H$, are calculated from the known experimental errors in the heat capacity (54) as

$$\sigma[S(T_n)_H] \cong 0.5\left\{\sigma C(T_1)_H + \sum_{i=1}^{n-1}\left[\left(\frac{\sigma C(T_i)}{T_i} + \frac{\sigma C(T_{i+1})}{T_{i+1}}\right)_H \times (T_{i+1} - T_i)\right]\right\}, \qquad 19.$$

where n is the number of heat capacity data points collected from the lowest temperature of experiment to a given temperature, T_n. Generally, the accuracy of the magnetocaloric effect calculated from heat capacity is much better than that from any other technique (direct or indirect magnetization) at low temperatures. Near room temperature, however, due to the accumulation of experimental errors in the total entropy functions (54), the errors in the magnetocaloric effect become approximately the same, 20 to 30%, as those from direct and magnetization data.

Special Problems—First Order Phase Transitions

If the magnetocaloric material undergoes a first order phase transition, any MCE measurement technique may potentially yield significantly inaccurate results if the source of the problem is not properly recognized. Direct measurements can easily yield an incorrect result if the transition has slow kinetics, as many first order materials do. Then, rapid magnetic field change required to fulfill adiabatic conditions

may not be slow enough to allow the transformation to proceed through the bulk of the sample. If more time is allowed for transformation to go to completion, the thermal isolation of the sample in the measurement equipment is usually not good enough, and the results can be considerably underestimated. One recent example is found in Reference 34, where the obviously erroneous direct measurements of the magnetocaloric effect in $Gd_5(Si_2Ge_2)$ alloy are treated without caution, and the authors make the wrong conclusions.

Indirect measurements are also not free from potential error, even though both magnetization and heat capacity are measured at nearly equilibrium conditions since magnetic field or temperature vary slowly. We note here that magnetization data are usually collected at constant temperature and in a slowly varying magnetic field, whereas heat capacity data are collected at constant magnetic field and with a slowly varying temperature. If the transition is sharp and proceeds at nearly ideal (theoretical) conditions, then the Maxwell equation (Equation 4) becomes invalid because both derivatives on the left and right hand sides of this equation become undefined. For the majority of materials, the transitions are not ideal (sharp enough), thus one can calculate both derivatives (Equation 4), and the use of the Maxwell equation remains valid.

The heat capacity data may yield the incorrect MCE near the first order phase transition because the non-zero enthalpy of transformation (i.e. the latent heat), combined with the non-zero heat capacity of the calorimeter sample holder, results in an unknown error in the experimental heat capacity measured in adiabatic heat pulse experiments (55). When this error is carried over into the MCE calculated using the measured heat capacity data (Equations 14–16), the MCE can suffer from large systematic errors. The deleterious effect of intrinsic errors of the heat capacity near the first order phase transition can be minimized by changing the experimental conditions during heat capacity measurements, or the entropy discontinuity can be determined (or refined) from different experimental data, such as magnetization or direct calorimetric measurements of ΔH_{tr}. When the entropy discontinuity is properly determined, the $S(T)_H$ functions calculated from heat capacity can be adjusted to reflect the proper ΔS_{tr}. Generally, if a material undergoes a first order phase transition, the magnetocaloric effect calculated from heat capacity should be compared with that measured directly under equilibrium conditions or calculated from magnetization data to ensure that the potentially deleterious effects of intrinsically inaccurate heat capacity have been eliminated or minimized (55).

LANTHANIDE (RARE EARTH)–BASED MATERIALS

For the remainder of this review, the magnetic field change is quoted in terms of:

$$\Delta H = H_F - H_I, \qquad 20.$$

where H_F is the final magnetic field, and H_I is the initial magnetic field, which is always 0 T unless noted otherwise.

Pure Metals

The magnetocaloric effect has been measured in one light lanthanide metal, polycrystalline Nd (56), and all of the heavy magnetic lanthanides, both polycrystalline and single crystal Gd (7, 24–27, 29, 33, 39, 48, 57–62), Tb (29, 60, 63–66), and Dy (24, 26, 33, 62, 67–69), and polycrystalline Ho (33, 62, 63, 66, 68, 70), Er (62, 66, 70, 71), and Tm (62, 66, 72).

Neodymium orders magnetically upon cooling at 19 and 8 K, which results in the double peak MCE structure (combination of the two caret-shaped peaks located at magnetic ordering temperatures), which was measured directly by Zimm et al (56) for $\Delta H = 1, 3, 5$, and 7 T. The maximum MCE is ~2.5 K at 8.5 K for $\Delta H = 7$ T. Both MCE and $RCP(T) = 54\ \mathrm{K}^2$ are quite low, indicating that the pure Nd metal is an unsuitable low-temperature magnetic refrigerant material.

Gadolinium is one of the most broadly studied magnetic refrigerant materials. It is ferromagnetic below 292 to 295 K depending on its purity, generally the cleaner metal orders at a higher temperature (24). The MCE in Gd has a normal caret-like shape behavior peaking at the Curie temperature despite the recent report (73) that it may not be actually ferromagnetic in low-magnetic fields below ~292 K. The MCE in Gd has been repeatedly measured directly and calculated from magnetization and heat capacity for very small (less than ~0.2 T) as well as for large ΔH (up to 10 T) by numerous groups. One obvious reason is that Gd is known to have the largest near room–temperature magnetocaloric effect (see Figures 2 and 4) and, therefore, is considered to be one of the best magnetic refrigerant materials for air conditioning and refrigeration. Its relative cooling power is impressive: $RCP(S)$ has values between ~2 and ~14 J/cm^3 for ΔH of 2 to 10 T, and the $RCP(T)$ values fall between ~240 and ~2000 K^2 for the same ΔH. Gadolinium plates ($\Delta H = 7$ T) were used in the first continuous near room–temperature magnetic refrigerator demonstrated by Brown (7), who attained a 47°C no-load temperature difference between the hot end (46°C) and cold end (−1°C) by regenerating a column of fluid (80% water and 20% ethyl-alcohol). Two magnetic refrigerator beds filled with ~3 kg of Gd powder (ΔH was varied between 1.5 and 5 T) were used by Zimm et al (22) in a proof-of-principle reciprocating device, which achieved 38°C temperature span and showed maximum cooling power of 600 W. The latter device demonstrated Carnot efficiencies in excess of 50% and a coefficient of performance (COP) in excess of 15. To date, pure Gd is one of the best magnetocaloric materials for the near room–temperature range (Figures 2 and 4) and is typically used for calibrations in any laboratory involved in magnetocaloric effect research.

Terbium orders antiferromagnetically on cooling at ~230 K, and then a first order phase transition from a helical antiferromagnetic to a ferromagnetic state occurs at ~221 K. Low magnetic field (ΔH less than 0.04 T) direct measurements indicate that the MCE in Tb is slightly negative around ~221 K, and it is positive

around ~231 K. In stronger magnetic fields, the MCE in Tb becomes a conventional caret-shaped peak with maximum at ~230 K and with a substantial cooling power. Its $RCP(T)$ reaches ~620 K^2 for a ΔH of 7 T, which is, however, more than twice as low as for Gd. All of the work on MCE in Tb was carried out using direct measurement techniques.

The complexity of the magnetic structure increases from Tb to Dy. The specifics of the magnetic structure and MCE in Dy were discussed above (see the section on Anomalous Magnetocaloric Effect and Figure 6). The maximum MCE occurs at ~180 K and the $RCP(T)$ in Dy reaches ~820 K^2 for a ΔH of 7 T. The MCE in Dy was studied independently using all three measurement techniques.

The magnetocaloric effect in Ho was measured directly only in high magnetic fields (ΔH of an order of 6 to 7 T). It was found to be relatively small and close to constant (~4 K between ~50, and ~140 K for a $\Delta H = 6$ T), which reflects the complex magnetic structure of the metal. The caret-shaped peak observed at ~130 K is heavily overlapped with a lower temperature, broad MCE maximum.

Pure Er has one of the most complex magnetic structures among heavy lanthanides. It orders antiferromagnetically upon cooling at ~86 K and then undergoes a first order magnetic phase transition from an antiferromagnet to a ferromagnet at ~19 K. Between these two temperatures several spin-slip transitions, as well as a change at ~52 K from a sinusoidally modulated to a basal spiral antiferromagnet, are observed. The MCE in Er was measured directly in magnetic fields up to 7.5 T, indicating almost constant value close to 4 K extending between ~25 and 100 K ($\Delta H = 7.5$ T). In lower magnetic fields, the MCE in Er becomes distinctly divided into two regions: the lower temperature broad maximum sharply rising at ~19 K and leveling off at ~70 K, and the overlapping caret-shaped peak at ~86 K (similar to that observed for Dy in $\Delta H = 2$ T; see Figure 5). Effects of both spin-slip transitions and modulated spiral antiferromagnet have practically no effect on the MCE in Er.

The magnetocaloric effect in Tm, which also orders in two steps, first antiferromagnetically at ~56 K and then ferromagnetically at ~20 K, was measured directly in magnetic fields corresponding to ΔH from 1 to 7 T. Similar to other heavy lanthanides, excluding Gd, the MCE in Tm is a combination of a caret-shaped peak observed at higher magnetic ordering temperature (when magnetic field becomes strong enough to quench the antiferromagnetism), and a broad low-temperature tail. The highest MCE in Tm (~3 K) is observed for $\Delta H = 7$ T.

Experimental studies of seven pure lanthanide metals indicate that Gd is the best magnetic refrigerant. This metal was already successfully used as a magnetic refrigerant to provide cooling between ~270 and ~310 K (7, 22). Other two lanthanides, Tb and Dy show somewhat lower MCE, but still can be used to provide magnetic cooling between ~210 and ~250, and ~160 and ~200 K, respectively. The operating temperature spans are given for ΔH between 5 and 7 T, which are feasible with superconducting magnet technology. If permanent magnets are used to provide magnetic field change, then ΔH is limited to ~2 T, and the useful temperature span of all three lanthanides decreases. Furthermore, Dy becomes

unusable because its MCE deteriorates rapidly in magnetic field below 2 T. All other magnetic lanthanides are obviously unusable as magnetic refrigerant materials because their MCE is too low.

Intra-Lanthanide Alloys

Introduction of alloying additions to the three best magnetocaloric lanthanides (Gd, Tb, and Dy) enables a considerable amount of freedom in adjusting the magnetic-ordering temperature and, therefore, the maximum MCE and the range of operating temperatures in the intra-lanthanide alloys. The gadolinium-based intra-lanthanide alloys have been studied with respect to their magnetocaloric properties most extensively. The following have been characterized: $Gd_{0.85}Y_{0.15}$ and $Gd_{0.85}Tb_{0.15}$ (74, 75); $Gd_{0.75}Y_{0.25}$ and $Gd_{0.48}Y_{0.52}$ (76, 77); $Gd_{0.52}Y_{0.48}$ (33); $Gd_{1-x}Tb_x$, where $x = 0.2$, 0.4, and 0.7 (78); $Gd_{1-x}Dy_x$, where $x = 0.12$, 0.28, 0.44, and 0.70 (79); $Gd_{1-x}Dy_x$, where $x = 0.1$, 0.2, and 0.3 (80); $Gd_{0.73}Dy_{0.27}$ (27); $Gd_{1-x}Ho_x$, where $x = 0.2$, 0.4, 0.6, and 0.8 (70); $Gd_{0.80}Ho_{0.20}$ (81); $Gd_{0.9}Er_{0.1}$ and $Gd_{0.69}Er_{0.31}$ (82); $Gd_{0.84}Er_{0.16}$ (81); and $Gd_{1-x}Er_x$, where $x = 0.2$, 0.4, 0.6, and 0.8 (70).

The addition of another lanthanide metal reduces the magnetic-ordering temperature of Gd and, generally, reduces the MCE. One of the most interesting results was reported by Shao et al (74, 75), who showed that $Gd_{0.85}Y_{0.15}$ nano-powders (average particle size 20 nm) display about a 10 to 15% increase of the MCE between 250 and ~300 K when compared with bulk alloy of the same stoichiometry (direct MCE measurements). This was associated with the superparamagnetic behavior of the nano-powders in contrast to the ferromagnetic behavior of the bulk alloy. Bulk $Gd_{0.75}Y_{0.25}$ and $Gd_{0.48}Y_{0.52}$ order ferromagnetically at 232 and 161 K, respectively. Both retain the normal caret MCE behavior, which is considerably reduced compared with that of pure Gd. The relative cooling power calculated from magnetization data is ~6 J/cm^3 and ~3.7 J/cm^3 in $\Delta H = 7$T for $Gd_{0.75}Y_{0.25}$ and $Gd_{0.48}Y_{0.52}$, respectively. Another, approximately equiatomic $Gd_{0.52}Y_{0.48}$ alloy has peak MCE of only ~3.8 K at ~162 K for $\Delta H = 7$ T.

The magnetocaloric effect in ΔH of 6 T in $Gd_{1-x}Tb_x$ alloys was measured directly, has the normal caret shape, and also shows a gradual decrease of both the value of MCE and the temperature of the maximum. Despite antiferromagnetism of pure Dy, the $Gd_{1-x}Dy_x$ alloys generally retain simple caret MCE behavior even at $x = 0.7$. The magnetic entropy change calculated from magnetization data by Smaïli & Chahine (79) indicates a nonliner behavior of the cooling capacity as a function of the Dy concentration (x) for $\Delta H = 7$ T: $RCP(S)$ varies from ~9 J/cm^3 at $x = 0$ to ~11 J/cm^3 at $x = 0.12$, and then ~8, ~11, and ~8 J/cm^3 for $x = 0.28$, 0.49, and 0.7, respectively. For a lower field change, $\Delta H = 1.6$. T Burkhanov et al (80) show that the reduction of the cooling capacity is small and gradual as the concentration of Dy increases from 0.1 to 0.3. Small additions of Ho and Er have almost no effect on the low field MCE of Gd (81), except they shift its ordering temperature to 263 and 260 K, respectively. When both Ho and Er are added in excess of 20 at%, the MCE of Gd (direct

measurements) continues shifting to lower temperatures, is considerably reduced, and its behavior deviates strongly from normal (70). The $Gd_{1-x}Ho_x$ and $Gd_{1-x}Er_x$ alloys display almost flat MCE when $x = 0.4$, which further transforms into double peak behavior for $x = 0.6$ and 0.8, closely resembling that of pure Ho and Er, respectively.

Tb-based intra-lanthanide alloys have been studied for $Tb_{1-x}Y_x$, where $x = 0.135$, 0.37, 0.9 (83) and $x = 0.09$, 0.165 (84, 85); and $Tb_{1-x}Dy_x$, where $x = 0.25$, 0.5, and 0.75 (86). Based on their direct measurements of $Tb_{1-x}Y_x$ single crystals, Nikitin & Tishin (83) report that when a ΔH of 6 T was applied along the *b*-axis, the MCE reaches ~7 K at 205 K for $x = 0.135$; 5.6 K at 177 K for $x = 0.37$, and MCE becomes virtually non-existent along both *b*- and *c*-axes for $x = 0.9$. Low magnetic field direct MCE measurements in $Tb_{0.91}Y_{0.09}$ indicate a ΔT_{ad} of ~0.5 K at 182 K ($\Delta H = 0.18$ T), and a ΔT_{ad} of ~0.5 K at 160 K ($\Delta H = 0.5$ T) in $Tb_{0.835}Y_{0.165}$ (84, 85). Weak magnetic field ($\Delta H = 1.3$ T) direct MCE measurements in $Tb_{1-x}Dy_x$ (86) show gradual transformation from normal caret-shape at $x = 0.25$ to a broad maximum followed by a skewed caret MCE peak at $x = 0.75$. The MCE value also gradually decreases in line with the differences between pure Tb and Dy.

Another intra-lanthanide alloy, $Er_{0.8}La_{0.2}$ was studied by Zimm (87). The introduction of La considerably changes the MCE behavior of Er. It becomes almost normal caret-shaped with a peak value of ~5.3 K at ~42 K in $\Delta H = 7$ T (measured directly). The relative cooling power, $RCP(T)$ remains low, reaching ~330 K^2 for $\Delta H = 7$ T.

Aluminides

By far, the lanthanide dialuminides have been the most extensively studied series of intermetallic compounds with respect to their magnetocaloric behavior. But two other aluminide phases have been investigated in addition to the RAl_2 phases. These are Gd_3Al_2 and Er_3AlC.

Gd_3Al_2 has been found to exhibit two widely separated ordering temperatures; a Néel temperature of 281 K and a Curie temperature of 39 K (88); as a result, this compound essentially has two non-overlapping caret-like magnetocaloric peaks. The ΔS_M value of the lower peak for a 10 T field change is higher than that of the upper peak, −58 versus −47 mJ/cm^3 K, whereas the adiabatic temperature rises are reversed, $\Delta T_{ad} = 3.5$ K at ~40 K and 7.1 K at ~280 K. Furthermore, the lower peak shifts significantly with increasing magnetic field from 39 K at 0 T to 50 K at 10 T, whereas the upper one remains essentially independent of the applied magnetic field.

The effect of carbon additions on the magnetic-ordering temperature and magnetocaloric effect of Er_3Al has been studied by Pecharsky & Gschneidner (89). They found that the ordering temperature is lowered from 9 K at $x = 0.1$ (Er_3AlC_x) to 5 K for $x = 1.0$, whereas the adiabatic temperature rise for a 10 T field change increased from 6 ($x = 0.1$) to 15.5 K ($x = 1.0$). The authors noted that all the samples

($x = 0.1$, 0.25, 0.5, 1.0) except $x = 1.0$ were two-phase materials consisting of Er_2Al and Er_3AlC. Er_3AlC was thought to order antiferromagnetically, but if so, the spins can be easily flipped by a low magnetic field (<2.5 T) because the magnetic field dependence of the heat capacity behaves like a ferromagnetic material. They concluded that all except $Er_3AlC_{0.1}$ could be used as low-temperature magnetic refrigerant materials.

The RAl_2 Laves phase compounds that have been studied for their magnetocaloric properties include both binary and ternary (pseudobinary) compounds $DyAl_2$ (26, 37, 90–93), $HoAl_2$ (90, 94), $ErAl_2$ (26, 37, 90, 92), $(Gd_{0.14}Er_{0.86})Al_2$ (95), $(Dy_{0.5}H_{0.5})Al_2$ (90), and $(Dy_{1-x}Er_x)Al_2$ (24, 26, 37, 77, 96). The MCE values of ΔS_M of $DyAl_2$ have been determined by Hashimoto et al (90) from magnetization and by Gschneidner et al (26, 37) from magnetization and heat capacity measurements, and in general the results from the two studies are in good agreement, i.e. $-\Delta S_M$ of 116 (90) and 110 mJ/cm^3 K (26, 37) for a 0 to 5 T field change and a $\delta_{FWHM} = 43$ K from both groups, in spite of the fact that the reported Curie temperatures are 8 K apart [55.9 K (90) and 63.9 K (26, 37)]. Földeaki et al (93) also determined ΔS_M from magnetization measurements for $\Delta H = 7$ T and reported a value of -135 mJ/cm^3 K for ΔS_M and a T_C of 56.1 K. Taking into account the difference in ΔHs, the MCE is essentially the same for all these groups. The $RCP(S)$ for $DyAl_2$ is quite large, about 5000 mJ/cm^3 [5010 (90) and 4750 (26, 37)]. Other studies on $DyAl_2$ indicate that only 23% of the theoretical entropy is utilized in the MCE for a field change of 7.5 T, which compares with 52% for $ErAl_2$ ($T_C = 13.6$ K) and 16% for $GdAl_2$ ($T_C = 167$ K) (91). The authors thought that the decrease in the utilized entropy with increasing T_C results from the increasing lattice contribution to the heat capacity with increasing ordering temperature, which would lead to a higher thermal load requiring more energy to heat the sample itself. Theoretical calculations of the influence of crystalline electric fields on the MCE were carried out on $DyAl_2$, $ErAl_2$, and $DyNi_2$ (92), and the authors showed that the calculated $-\Delta S_M$ and ΔT_{ad} values were in good agreement with experiment.

The MCE for $HoAl_2$ was reported by Hashimoto et al (90); Daudin & Bonjour (94) measured the heat capacity at 0, 2, 4, 6, and 8 T and presented entropy versus temperature curves but derived neither ΔT_{ad} nor ΔS_M. The MCE values are $\Delta S = -156$ mJ/cm^3 K, $\delta T_{FWHM} = 26$ K, and $RCP(S) = 4200$ mJ/cm^3 at $T_C = 28$ K for a 5 T field change (90). These values, as one might expect, fall between those of $DyAl_2$ and $ErAl_2$. A $\Delta T_{ad} = 12$ K was estimated from the entropy curves (94) at the Curie temperature of 33 K, which is 5 K higher than that given by Hashimoto et al (90).

Both ΔT_{ad} and ΔS_M have been reported for $ErAl_2$ by Hashimoto et al (90) using a direct measurement and magnetization studies, respectively, and by Pecharsky, Gschneidner and co-workers (26, 37) using heat capacity and magnetization methods. The results reported by the two groups are in fair agreement: The former give $T_C = 11.7$ K, $\Delta T_{ad} = 9.4$ K, $\Delta S_M = -215$ mJ/cm^3 K, and $RCP(S) = 3440$ mJ/cm^3 for a $\Delta H = 5$ T; for the same field change the latter give $T_C = 13.6$ K,

$\Delta T_{ad} = 11.1$ K, $\Delta S_M = -241$ mJ/cm^3 K, and $RCP(S) = 3610$ mJ/cm^3. The latter values are probably the more reliable because these authors used a higher purity Er metal to prepare their $ErAl_2$ materials.

Several ternary (R, R′)Al_2 phases, where R and R′ are different lanthanide metals, have been investigated. Zimm et al (95) studied $(Gd_{0.14}Er_{0.86})Al_2$ using heat capacity measurements. The zero field heat capacity showed two small rounded peaks at ~15 and 30 K, which gave a rounded magnetocaloric peak at 23.5 K, $\Delta T_{ad} = 8.9$ K, and $\delta T_{FWHM} = 42$ K for a $\Delta H = 7$ T. The ΔS_M values were not reported by the authors.

Hashimoto et al (90) determined the MCE of $(Dy_{0.5}Ho_{0.5})Al_2$ using magnetization data. They reported $\Delta S_M = -133$ mJ/cm^3 K, $\delta T_{FWHM} = 36$ K, and $RCP(S) =$ 4200 J/cm^3 for a 5 T field change. The MCE values for these two ternary alloys are consistent with those observed in the binary RAl_2 (R = Dy, Ho, Er) and the $(Dy_{1-x}Er_x)Al_2$ alloys.

A series of pseudo-binary $(Dy_{1-x}Er_x)$ Al_2 alloys were studied by Gschneidner and co-workers (24, 26, 36, 37, 96) using magnetic susceptibility, dc magnetization and heat capacity measurements, whereas Földeaki et al (77) studied the $(Dy_{0.5}Er_{0.5})Al_2$ composition. The Curie temperatures decrease linearly with increasing x from 63.9 for $DyAl_2$ to 13.6 K for $ErAl_2$, except for $x = 0.25$, which shows a slight dip from the straight line established by the other compositions (37). As is seen in Figure 3*a*, the ΔT_{ad} and ΔS_M values have an inverse dependence on x; they are the largest for $ErAl_2$ and decrease in a fairly smooth fashion to $DyAl_2$. The $RCP(S)$ and $RCP(T)$ values shown in Figure 3*b* exhibit an unusual trend in view of the x dependence of ΔT_{ad} and ΔS_M. This suggests the δT_{FWHM} is an important quantity in determining the cooling capacity of a material, and may have a bigger impact than the maximum ΔS_M or ΔT_{ad} (see Equations 10 and 11). Because of a spin re-orientation transformation in some of these $(Dy_{1-x}Er_x)Al_2$ alloys, special care must be used when evaluating the MCE properties from heat capacity data (26). As the authors have shown, this is one case where determining the MCE properties by another technique (magnetization) proved to be critical and helped to avoid reporting erroneous data. Gschneidner et al (36, 96) suggested that $(Dy_{0.5}Er_{0.5})Al_2$ might be a useful alloy as an active magnetic regenerator material in a magnetic refrigerator for liquefying hydrogen gas. Földeaki et al (77) noted that the MCE (ΔS_M) was increased by ~10% by grinding a $(Dy_{0.5}Er_{0.5})Al_2$ alloy relative to the as cast material.

GdPd

GdPd, which orders at 40 K, has been extensively studied for its MCE properties (24, 26, 36, 95–97), and it serves as a low-temperature standard against which the properties of other materials, which order magnetically between 25 and 55 K, are compared. Barclay et al (97) was the first to report on the MCE properties of GdPd. Based on zero field and 5 T heat capacity data, they reported a value of $\Delta T_{ad} = 9.0 \pm 1.0$ K for a 5 T field change at 37.5 K (they gave $T_C = 40$ K). In

view of more recent data, this value seems to be too high by about 30%. Zimm et al (95) measured ΔT_{ad} directly and obtained a value of 7.0 K for a $\Delta H = 5$ T, and this was confirmed by Pecharsky et al (24, 26), who obtained a value of 6.8 K (26) and 6.7 K (24) from two different sets of heat capacity measurements. Other values have been reported for larger magnetic field changes: for a 7 T field change, $\Delta T_{ad} = 8.7$ K (95); for a field change of 7.5 T, $\Delta T_{ad} = 9.6$ K (36, 96), while later measurements by the same group (24) reported a significantly lower value of $\Delta T_{ad} = 8.6$ K for this same ΔH; and for a 10 T field change, $\Delta T_{ad} = 10.1$ K (24). Although the heat capacity as a function of magnetic field and temperature has been measured three times, ΔS_M values have not been reported.

Gadolinium Silicides

The pseudo-binary system Gd_5Si_4–Gd_5Ge_4 is the only silicide system studied with respect to its magnetocaloric properties. Three different phase regions exist in the $Gd_5(Si_xGe_{1-x})_4$ alloys (98). The binary Gd_5Si_4 is orthorhombic, and almost 50% of Si can be substituted by Ge without a change in the crystal structure and with little change in the magnetocaloric properties of the materials (40, 98). The $Gd_5(Si_xGe_{1-x})_4$ alloys with $0.5 < x \leq 1.0$ are ferromagnetic and order magnetically between ~336 K ($x = 0$) and ~300 K ($x = 0.515$) and display conventional magnetocaloric behavior (99). The MCE and cooling capacity are 5 to 20% lower than that of Gd; however, all alloys from this phase region order magnetically at temperatures higher than that of pure Gd despite almost 45 at% dilution by nonmagnetic Si and Ge atoms (98). A summary of the ordering temperatures and magnetocaloric properties are listed in Table 1.

When the concentration of Ge in the $Gd_5(Si_xGe_{1-x})_4$ alloys increases to $0.24 \leq x \leq 0.5$, 50% of the Si(Ge)-Si(Ge) covalent bonds are broken, which causes a change of the crystal structure from the room-temperature orthorhombic Gd_5Si_4-type to the room-temperature monoclinic $Gd_5(Si_2Ge_2)$-type (98). This change is accompanied by drastic changes of magnetic and magnetocaloric properties of these alloys when compared with $0.5 < x \leq 1.0$ (see Table 1) (39, 40, 42). The temperature and magnetic field–induced transition from a paramagnetic to a ferromagnetic state in these alloys is a simultaneous first order magnetic and crystallographic transformation (100). The observed ΔS_M values become several times larger than those in any other known magnetocaloric material, thus leading to a giant magnetocaloric effect in all alloys with $0.24 \leq x \leq 0.5$. When direct MCE measurements were carried out under non-equilibrium conditions (34), at least for the $Gd_5(Si_2Ge_2)$ composition, the result was erroneous and MCE was underestimated, thus supporting the conclusion that the giant magnetocaloric effect is due to a first order phase transition in this alloy.

When the amount of Ge in the $Gd_5(Si_xGe_{1-x})_4$ alloys increases to $0 \leq x \leq 0.20$, the remaining Si(Ge)-Si(Ge) covalent bonds are broken, which causes a second change of the crystal structure from a room-temperature monoclinic $Gd_5(Si_2Ge_2)$-type to a room-temperature orthorhombic Gd_5Ge_4-type (98). Magnetic and

TABLE 1 The magnetic ordering temperature and magnetocaloric properties of the $Gd_5(Si_xGe_{1-x})_4$ phases[a]

Composition	T_C (K)	T_N (K)	$-\Delta S_M$ (mJ /cm^{3}K)	δT_{FWHM} (K)	ΔT_{ad} (K)	ΔH (T)	$RCP(S)$ (mJ /cm^3)
Orthorhombic							
Gd_5Si_4	336	–	61.7	72	8.8	5	4442
$Gd_5(Si_{3.5}Ge_{0.5})$[b]	331	–	55.0	64	7.3	5	3520
$Gd_5(Si_3Ge_1)$[b]	323	–	65.3	68	8.6	5	4440
$Gd_5(Si_{2.5}Ge_{1.5})$[b]	313	–	70.7	66	8.5	5	4666
$Gd_5(Si_{2.06}Ge_{1.94})$	306	–	70.5	68	8.0	5	4794
Monoclinic							
$Gd_5(Si_2Ge_2)$	276	–	140	24	15.0	5	3360
$Gd_5(Si_{1.72}Ge_{2.28})$	246	–	298	14	18.8	5	4172
$Gd_5(Si_1Ge_3)$	140	–	538	9	11.8	5	4840
$Gd_5(Si_{0.9}Ge_{3.1})$[c]	130	–	240	20	10.5	5	4800
Orthorhombic							
$Gd_5(Si_{0.8}Ge_{3.2})$	121	135	166	20	9.2	5	3320
$Gd_5(Si_{0.33}Ge_{3.67})$[c]	68	128	287	21	11.2	5	6027
$Gd_5(Si_{0.15}Ge_{3.85})$	40	127	177	25	8.8	5	4425
Gd_5Ge_4	20	125	128	27	7.2	5	3456

[a]From References 39, 40, 42, 99.

[b]Unpublished information. AO Pecharsky, Ames Laboratory, Ames, Iowa.

[c]KA Gschneidner Jr & VK Pecharsky, unpublished results.

magnetocaloric properties change again, but the giant magnetocaloric effect is preserved in all alloys with $0 \leq x \leq 0.20$ (see Table 1). The transition apparently remains a first order transformation, but its mechanism presently remains unclear.

Besides the large magnetocaloric effect, two additional features make $Gd_5(Si_xGe_{1-x})_4$ alloys unique and likely candidate magnetic refrigerant materials for the use in highly efficient magnetic refrigerators. The first is the fact that their Curie temperature can be tuned between ~20 K and ~336 K by varying the Si to Ge ratio (40). This in turn allows one to tune the maximum magnetocaloric effect between ~20 and ~336 K. The second is the fact that, unlike FeRh (see below), the giant magnetocaloric effect in the $Gd_5(Si_xGe_{1-x})_4$ alloys, where $0 \leq x \leq 0.5$, is reversible, i.e. it does not disappear after the first application of the magnetic field as occurs in FeRh. The difference in the behavior of the MCE in FeRh and $Gd_5(Si_xGe_{1-x})_4$ alloys is most likely associated with the difference in the nature of the first order phase transition, which in the former case is a magnetic order-order transformation, whereas in the latter case it is a simultaneous magnetic and crystallographic phase transition, i.e. it is a magnetic order-disorder and a crystallographic order-order phase transformation.

Unfortunately, substitution of small amounts of both Si and Ge by Al, Fe, Co, Ni, Cu, and C in the $Gd_5(Si_2Ge_2)$ alloys destroys the first order magnetic phase transition and the giant magnetocaloric effect, although the MCE remains quite large, larger than in any other material except pure Gd and several Gd-R alloys (41). Addition of small amounts of Ga, i.e. $Gd_5(Si_{1.985}Ge_{1.985}Ga_{0.03})$, to the $Gd_5(Si_2Ge_2)$ alloy, however, not only preserves the giant magnetocaloric effect, but also raises the temperature of the first order phase transition by ~10 K, from ~276 to ~286 K (41), thus extending the range of the giant magnetocaloric effect. More studies are needed to fully understand the effects of various alloying additions on the first order phase transition in $Gd_5(Si_xGe_{1-x})_4$ alloys, where $0 \leq x \leq 0.5$.

EuS

The MCE properties of EuS were reported by Hashimoto et al (31, 101). Because Eu is divalent in EuS, it has a $4f^7$ configuration, the same as trivalent Gd, and thus it might be expected to have good MCE properties. Indeed, this is the case; $\Delta S_M = -364$ mJ/cm^3 K at $T_C = 16$ K for a 10 T field change, which is larger than that of $(Dy_{0.1}Er_{0.9})Al_2$ ($\Delta S_M = -250$ mJ/cm^3 K and $T_C = 17.7$ K) for the same field change. The $RCP(S)$ is also quite large: 8730 mJ/cm^3 [for $(Dy_{0.1}Er_{0.9})Al_2$ it is 8010 mJ/cm^3]. Thus it would appear that EuS would be an effective magnetic refrigerant below 20 K.

Zinc Alloys

Shao et al (74, 75) prepared nano-size amorphous powders of a $Gd_{0.75}Zn_{0.25}$ alloy by rapid solidification followed by ball-milling to 360 nm. Some of these powders were rolled into ribbons (bulk). They measured the ΔT_{ad} directly for the powder and bulk materials for $\Delta H = 1$ T. The nano-size powder had a broad maximum at 287 K with a $\Delta T_{ad} = 1.1$ K, whereas the bulk sample had a rounded maximum at 299 K with a $\Delta T_{ad} = 2.2$ K. The value for the bulk material is ~50% lower than that of pure Gd metal (see Figure 2*b* and/or Figure 4) for the same field change.

The MCE properties of GdZn and several two-phase mixtures of GdZn and Gd containing different proportions of the two phases were reported by Pecharsky & Gschneidner (102). The MCE properties of GdZn with $T_C = 270$ K are $\Delta S_M = -85.9$ mJ/cm^3 K, $\Delta T_{ad} = 10.6$ K, and $RCP(S) = 11{,}160$ mJ/cm^3 for a 10 T field change. These properties are ~30% smaller than those of pure Gd metal. The authors showed that a two-phase mixture of Gd + GdZn can be used as effective active magnetic regenerator material, because by changing the ratios of the two components, the profile of the ΔS_M versus T and the ΔT_{ad} versus T behaviors can be changed or adjusted to more nearly match the desired behavior for the thermodynamic cycle chosen for a particular refrigeration/cooling application.

ErAgGa

The MCE of ErAgGa was determined from low-temperature heat capacity measurements as a function of magnetic field (89). The adiabatic temperature rise,

$\Delta T_{ad} = 11.5$ K for a 10 T field change, is about 50% smaller than that of Er_3AlC, which orders ferromagnetically at 3.1 K. The smaller value is probably due to the fact that ErAgGa forms a low temperature (3 to 5 K) nonmagnetic atom disordered (NMAD) spin glass system.

3*d* TRANSITION METAL–BASED MATERIALS

3*d* Metals

The magnetocaloric effect, ΔT_{ad}, has been measured in Fe, Co, and Ni at their respective Curie points, 1042 K (769°C), 1386 K (1113°C), and 633 K (360°C). They all exhibit normal caret-like magnetocaloric peaks. The magnetocaloric effect in Fe has been measured in three magnetic fields of up to 0.8 T by Potter (103) and at 3.0 T by Hirschler & Rocker (104); in Co in 10 different magnetic fields of up to 2.32 T by Rocker & Kohlhaas (105); and in Ni in four different magnetic fields of up to 1.50 T by Weiss & Piccard (106), in four fields of up to 1.78 T by Weiss & Forrer (107), at 3.0 T by Hirschler & Rocker (104), and at 1.78 T by Hashimoto et al (31). The maximum ΔT_{ad} values reported are 5.2 K at 3.0 T (104) and 2.0 K at 0.8 T (103) for Fe; 3.25 K at 2.32 T (105) for Co; and 1.8 K at 3.0 T (104), 0.57 K at 2.50 T (106), 1.26 K at 1.78 T (107), 1.32 K at 1.78 T (31), and 0.13 K at 0.09 T (108) for Ni.

It is difficult to make a meaningful comparison of these values because the measurement field varies considerably—between 0.8 and 3.0 T. However, comparing the rate of change of ΔT_{ad} per tesla one can see a trend developing, keeping in mind that ΔT_{ad} versus the magnetic field, as shown earlier, is not a linear function, but decreases as the field increases. For Fe the values are 2.5 and 1.7 K/T; for Co 1.4 K/T; and for Ni 0.60, 0.38, 0.71, 0.74, and 1.4 K/T, respectively. The high value (1.4 K/T) reported by Noakes & Arrott (108) for very small field changes in Ni is not at all unreasonable since the rate of change of the MCE decreases with increasing field. In the case of Ni, the magnetocaloric effect reported by Weiss & Piccard (106) is probably in error (it is about half of the other three values). Averaging the values we have 2.1 K/T for Fe, 1.4 K/T for Co, and 0.68 K/T for Ni (discarding the values of Weiss & Piccard, and Noakes & Arrott). The values are consistent with the trend of the effective magnetic moments of Fe (2.22 μ_B), Co (1.72 μ_B), and Ni (0.61 μ_B) (109).

The adiabatic temperature rise for Fe is quite large when one considers that the field dependence of ΔT_{ad} is 2.4 K/T for a 5.0 T field for Gd, which has an effective moment of 7.94 μ_B at its Curie temperature of 294 K. It is also reasonable to assume that the relatively large ΔT_{ad} in Fe is associated with a large increase of T/C_p (see Equation 9), and therefore the apparent reduction of $\partial M/\partial T$ compared with that in Gd is practically offset by a nearly threefold increase in T provided C_p remains about the same for both Fe and Gd near their T_Cs.

Another measure of the cooling power, as noted above, is the product of the adiabatic temperature rise and the peak width at half the peak height ($\Delta T_{ad} \times \delta T_{FWHM}$)

RCP(T), i.e. relative cooling power for a given magnetic field. The *RCP*(T) values are 286 K^2 for Fe at 3.0 T, 182 K^2 for Co at 2.32 T, and 63 K^2 for Ni at 3.0 T. These numbers are also consistent with the ΔT_{ad} trend noted above, despite the value for Co being for a field of 2.3 T, which is 0.7 T less than that for Fe and Ni. The corresponding value for Gd at 3.0 T is 365 K^2, which is significantly larger than those of Fe by virtue of its larger ΔT_{ad} value (7.3 versus 5.2 K).

Although their *RCP*(T) values are lower than those of Gd, which is known to be an efficient magnetic refrigerant (22), both Fe and Co should be reasonably effective for magnetic cooling or heating applications in the vicinity of their Curie temperatures. As far as we are aware, the ΔS_M magnetocaloric effect values have not been calculated for any of these 3*d* metals.

3*d* Metal–Based Alloys and Intermetallic Compounds

The magnetocaloric effect of a solid solution alloy of Si in Fe, $Fe_{0.9357}Si_{0.0643}$ has been measured directly by Hirschler & Rocker (104). For a magnetic field change of 3 T, the magnetocaloric effect has basically a normal caret-shape peak, with a maximum of 5 K observed at 1013 K, which is slightly lower than that of pure Fe ($\Delta T_{ad} = 5.2$ K at 1042 K). Below the Curie temperature, the MCE behavior displays a shoulder at 973 K. The relative cooling power between 983 and 1043 K is quite large, *RCP*(T) = ∼300 K^2.

Another solid solution alloy, $Mn_{0.225}Cu_{0.775}$, has been studied by Znamenskii & Fakidov (110). The MCE in this alloy has been measured directly between 77 and ∼130 K in magnetic fields from 0.13 to 1.38 T. For ΔH larger than 0.42 T, the MCE is positive down to 77 K, but for smaller magnetic fields, the MCE becomes negative at the lowest temperature of the experiment, which indicates the presence of antiferromagnetic interactions in $Mn_{0.225}Cu_{0.775}$. Except for the negative sign, the MCE in $Mn_{0.225}Cu_{0.775}$ has normal caret behavior peaking at 95 K ($\Delta T_{max} = 0.145$ K for $\Delta H = 1.38$ T) with a very low relative cooling power *RCP*(T) = ∼3.6 K^2 between 83 and 108 K.

Several 3*d*-based intermetallic compounds, $Mn(As_{1-x}P_x)$, $Ni_2(Mn_{1-x}V_x)Sn$, $Ni_2(Mn_{1-x}Nb_x)Sn$, $Mn_{3-y-x}Cr_yAlC_{1+x}$, $(Hf_{0.83}Ta_{0.17})Fe_{2+x}$, FeRh, and Cr_3Te_4 have been investigated with respect to their magnetocaloric properties. Kuhrt et al (111) report direct MCE measurements for $Mn(As_{1-x}P_x)$ in magnetic fields up to 7 T. In low magnetic fields (below 3 T), the MCE for both $x = 0.09$ and 0.08 shows a double-peak behavior consistent with an antiferromagnetic ground state and a magnetic field–induced metamagnetism, but when the magnetic field is increased to 7 T, the MCE behavior becomes conventional. In a 7 T magnetic field, the MCE maximum occurs at ∼225 K and ∼233 K in $Mn(As_{0.92}P_{0.08})$ and $Mn(As_{0.91}P_{0.09})$, respectively, with ΔT_{ad} peaking around 1.3 K. The relative cooling power for $\Delta H = 7$ T is quite low: *RCP*(T) for both alloys is approximately 70 K^2.

The magnetocaloric effect in two series of alloys, $Ni_2(Mn_{1-x}M_x)Sn$ (where M = V, Nb, and $x = 0.1$, 0.2, 0.3, 0.4) and $Mn_{3-y-z}Cr_yAlC_{1+z}$ (where $y = 0$, $z = -0.16$, -0.08, 0, and $z = 0.1$, and $y = 0$, 0.06, 0.15, 0.26), has been measured

indirectly (magnetization) by Maeda et al (112). Low magnetic field (1.4 T) measurements indicate that the Curie temperature in the series $Ni_2(Mn_{1-x}V_x)Sn$ is lowered from ~305 to ~160 K as x increases from 0.1 to 0.4. The MCE in these alloys exhibits conventional behavior, and the relative cooling power also decreases from ~440 mJ/cm^3 ($x = 0.1$) to ~350 mJ/cm^3 ($x = 0.3$) and then increases to ~400 mJ/cm^3 for $x = 0.4$ for $\Delta H = 1.4$ T. When the magnetic field is increased to 7 T, the $RCP(S)$ for $Ni_2(Mn_{0.8}V_{0.2})Sn$ also increases to ~2.4 J/cm^3.

The temperature of the maximum MCE decreases from ~300 K to ~190 K in a series of $Mn_{3-y-z}Cr_yAlC_{1+z}$ alloys, where $y = 0$, $z = -0.08$; $y = 0$, $z = 0$; $y = 0$, $z = 0.1$; $y = 0.06$, $z = 0.1$; $y = 0.15$, $z = 0.1$; and $y = 0.26$, $z = 0.1$. They all exhibit the normal MCE behavior, the maximum $RCP(S)$ is ~580 mJ/cm^3 for $y = 0$, $z = -0.08$, and the minimum, ~360 mJ/cm^3, is observed at $y = 0.26$, $z = 0.1$. For comparison, the $RCP(S)$ in Gd for $\Delta H = 1.4$ T is ~890 mJ/cm^3.

Herbst et al (113) reported the indirect MCE (magnetization) for low magnetic fields (0.9 T) in the three $(Hf_{0.83}Ta_{0.17})Fe_{2+x}$ alloys, where $x = 0.09$, 0, and -0.09. All three materials order antiferromagnetically near room temperature and have a relatively low MCE (-5.6, -16, and -11 mJ/cm^3 K, respectively), which shows almost conventional behavior. The relative cooling power, $RCP(S)$, is quite low totaling at ~178, ~247, and ~254 mJ/cm^3 for $x = 0.09$, 0, and -0.09, respectively. Although no quantitative MCE data are given, Herbst et al mention that at $x = -0.02$ the sharpness of the magnetic phase transition indicates the possibility of the giant magnetocaloric effect with $-\Delta S_M$ exceeding 220 mJ/cm^3 K.

The intermetallic FeRh is the first known intermetallic material reported to display the giant magnetocaloric effect near room temperature (43, 45). Direct measurements of the MCE of a heat-treated and quenched $Fe_{51}Rh_{49}$ alloy (43) indicated that it could be as large as -13 K at 307 K in a magnetic field of 1.95 T, but later (45) it was reported to be -8.2 K for $\Delta H = 2.5$ T. The MCE behavior in this material is unusual because of its sign (it is negative for a positive ΔH), its extreme sensitivity to processing history, and its irreversibility. The MCE in FeRh displays an inverse skyscraper behavior with the large relative cooling power, $RCP(T)$, of -166 K^2 between 296 and 316 K.

The compound Cr_3Te_4 displays a conventional MCE (measured directly), which reaches 1.1 K at 316 K in 2 T magnetic field (31). The relative cooling capacity, $RCP(T) = 41$ K^2 is quite low.

The limited amount of available experimental data indicates that, in general, the MCE in transition metal–based alloys is lower than that in lanthanide-based alloys for the same temperature range. This is consistent with the lower available theoretical magnetic entropy in the magnetic transition metal atoms. This makes them unlikely candidates for use as magnetic refrigerant materials below ~300 K, but they may be useful materials for magnetic refrigerators/heat pumps rejecting heat well above room temperature. However, if new 3*d*-based alloys are found, with a giant MCE similar in magnitude to that observed in FeRh, but reversible, they could be an excellent source of highly effective magnetic refrigerant materials.

MIXED LANTHANIDE–3*d* TRANSITION METAL COMPOUNDS

Manganese-Based Intermetallics

The ternary compound $NdMn_2Si_2$ has been reported to order magnetically at 32 K with a magnetocaloric effect, ΔT_{ad}, of 8.4 K for a field change of 0 to 6 T (114). This value is comparable to that observed in $(Dy_{0.4}Er_{0.6})Al_2$, which orders at 31.6 K [$\Delta T_{ad} = 10.4$ K for a field change of 0 to 7.5 T] (37), when considering the differences in the magnetic field [i.e. ΔT_{ad} per T is 1.4 K/T for the $NdMn_2Si_2$ versus 1.39 K/T for the $(Dy_{0.4}Er_{0.6})Al_2$ phase]. Just below the Curie temperature ($\sim$28 K) a small negative ΔT_{ad} peak was observed at high magnetic field (>3 T). The magnitude of $|\Delta T_{ad}|$ increased with increasing field, and the peak temperature shifted to lower temperatures. For a 6 T field, the peak occurred at 26 K with a $\Delta T_{ad} = -0.44$ K.

Iron-Based Intermetallics

The adiabatic temperature rise was measured for YFe_2, $ErFe_2$, YFe_3, and $HoFe_3$ for a magnetic field change of 1.58 T by Nikitin et al (115). The YFe_2 and YFe_3 phases exhibited a small caret-like magnetocaloric effect of 1.25 and 1.42 K at 530 and 533 K, respectively. The magnetocaloric effect for $ErFe_2$ and $HoFe_3$ is more complex because there are two magnetic sublattices, the lanthanide and the iron, that are orientated antiparallel to each other and order at substantially different temperatures. The lanthanide ions order at $\sim$330 K for both $ErFe_2$ and $HoFe_3$, whereas the Fe ions order at 575 and 571 K, with a compensation temperature of 490 and 389 K, respectively. These behaviors give rise to a small broad positive ΔT_{ad} of 0.20 and 0.18 K at the respective Er and Ho magnetic lattices' ordering temperatures ($\sim$330 K); a small sharp negative ΔT_{ad} of -0.10 and -0.11 K at the respective compensation temperature (490 and 389 K); and a small sharp peak for ΔT_{ad} (0.31 and 0.56 K) at iron magnetic lattice ordering temperatures, 575 and 571 K, respectively. For the YFe_2 and YFe_3 phases the magnetocaloric effect is about the same as that of Ni metal ($\Delta T_{ad} = 1.26$ K for $\Delta H = 1.78$ T), which orders about 50 K higher than the two Fe intermetallic compounds.

The magnetocaloric effect was measured for a series of $TbFe_2$-YFe_2 alloys by Nitikin et al (116), (see Table 2). As is evident, the Curie temperatures increase in more or less a linear fashion from YFe_2 to $TbFe_2$, while the magnetocaloric properties decrease from both end members, reaching a minimum at $x = 0.45$. This behavior is due to several factors. One is that the effective magnetic moment on Fe increases from 1.44 μ_B for YFe_2 to 1.7 μ_B for $TbFe_2$. In addition, below the compensation temperatures the Tb ions are aligned with the applied magnetic field while the Fe spins are antiparallel. As the magnetic field is increased the magnetic moments on the Tb lattice increase and those on the Fe lattice decrease; above the compensation temperature the opposite occurs. Finally, when one takes into

TABLE 2 Magnetic ordering and compensation temperatures, and magnetocaloric properties of some $(Tb_xY_{1-x})Fe_2$ alloys for a magnetic field change of 0 to 1.5 T (116)

Composition x	T_c (K)	ΔT_{ad} (K)	δT_{FWHM} (K)	$RCP(T)$ (K^2)	$T_{comp.}$[a] (K)
0	528	1.29	27	34.8	–
0.20	575	0.70	36	25.2	400
0.33	595	0.43	40	17.2	250
0.45	618	0.21	30	6.3	450
0.80	665	0.51	30	15.3	–
1.00	697	0.72	20	14.4	–

[a]Compensation temperature

account the concentration changes as x varies, the magnetic moment on the Tb sublattice is found to be equal to that of the iron sublattice when $x = 0.5$. In any event the magnetocaloric properties are relatively small, even for $x = 0$ and 1.0.

Cobalt-Based Intermetallics

The cubic Laves phases $DyCo_2$, $HoCo_2$, and $ErCo_2$ have been studied for their magnetocaloric properties. All three phases exhibit a first order magnetic/structural transition. $DyCo_2$ orders at 142 K, but its ΔS_M MCE peak is rounded and much broader than one would expect for a first order transition, even broader than that for a typical second order magnetic phase transition (93). $\Delta S_M = -150$ mJ/cm^3 K, $\delta T_{FWHM} = 34$ K and $RCP(S) = 5{,}100$ mJ/cm for a field change of 7 T (93).

$HoCo_2$ orders at 83 $\pm$ 1 K, which shifts to high temperatures with increasing magnetic field (117). The adiabatic temperature rise is somewhat small, 5.1 K for a 6 T field change, and the magnetocaloric peak is not particularly sharp for a first order transition, especially on the high-temperature side where it falls off rather slowly. This behavior may be due to the metamagnetic character reported for this phase. For small magnetic field changes (<0.5 T), a small negative ΔT_{ad} (~ -0.5 K) was observed below the Curie temperature, but for field changes 2.0 T or greater, the negative adiabatic temperature change is no longer evident (117). The ΔS_M was calculated by Földeaki et al (93) and its value (-224 mJ/cm^3 K for a $\Delta H = 7$ T) is consistent with the ΔT_{ad}. The shape of the ΔS_M versus T is somewhat broader than the typical caret-shaped peak, especially so considering the rounded peak shape.

$ErCo_2$ also exhibits a first order magnetic/structural transition at 31 K, which shifts to high temperatures with increasing applied magnetic field, i.e. it is 46 K at 7 T and 54 K at 14 T (93, 118). The ΔS_M values were obtained from both magnetization and heat capacity measurements, and the agreement was only fair. For example the peak values were 298 (93, 118) and 334 mJ/cm^3 K (118), respectively, while the temperatures of the peaks were $\sim$12 K apart (41.5 and 34 K, respectively). The shapes were distinctly different, the ΔS_M values from magnetization

measurements rose rapidly on the low-temperature side of the peak, typical of a first order transition, remained somewhat constant for almost 5 K before they fall off with a caret-like shape on the high-temperature side of the peak (118). The adiabatic temperature rise as determined from heat capacity has a shape similar to the ΔS_M peak derived from the heat capacity, as one might expect. The value of ΔT_{ad} is 12 K for a 7 T field change, which is better than that of $HoCo_2$ (see above) and that of $(Dy_{0.4}Er_{0.6})Al_2$, 10.4 K for a 7.5 T field change at its Curie temperature of 31.6 K. The authors (118) believe the discrepancy between the heat capacity and magnetization measurements for the magnetocaloric properties arises because "the boundary conditions used in the derivation of the approximate formula for simple ferromagnetic materials are not appropriate for more complex transitions as in $ErCo_2$."

Nickel-Based Intermetallics

The heat capacity of Er_3Ni, which orders at 6 K, was measured at 0, 1, 3 and 4.3 T from ~4 to 20 K by Tokai et al (119). The entropy versus temperature curves for each field were derived and plotted, but no ΔS_M or ΔT_{ad} values were reported. We have estimated from these graphs that $\Delta S_M = 95$ mJ/cm^3 K and $\Delta T_{ad} = 3$ K at 6 K for a 4.3 T field change, which are reasonable but not outstanding values.

The adiabatic temperature rise, ΔT_{ad}, of GdNi was determined by Zimm et al (95) from direct measurements at T_C (71 K) to be 7.4 K for a magnetic field change of 7 T, which is a reasonable value. They also measured ΔT_{ad} for field changes of 1, 3, and 5 T. The curves are typical caret-like for all four field changes.

The MCE values have been measured for a number of the RNi_2 phase with R = Gd, Tb, Dy, Ho, Er and $Gd_{0.1}Dy_{0.9}$. Zimm et al (95) determined δT_{ad} for $GdNi_2$ ($T_C = 75$ K) for field changes of 1, 3, 5, and 7 T. The ΔT_{ad} values are not particularly large (5.81 K for the largest field change), but the peaks are rather broad, and still retain the caret-like peak shape. Földeaki et al (93) calculated ΔS_M using magnetization measurements and also found it to be significantly smaller than that of several other RNi_2 or RCo_2 phases, which is consistent with Zimm et al's observation. They (93) reported $GdNi_2$ to have a $T_C = 70$ K, and $\Delta S_M = -137$ mJ/cm^3 K for $\Delta H = 7$ T. The peak was somewhat broad ($\delta T_{FWHM} = 44$ K), and the resultant $RCP(S)$ was slightly larger than those of $HoCo_2$ and $ErCo_2$ but significantly less than that of $DyNi_2$.

$TbNi_2$ which orders ferromagnetically at 38 K, exhibits a ΔT_{ad} value of 11 K for a 0 to 7.5 T field change according to Gschneidner et al (96), as determined from the heat capacity measurements. This value is about twice that of $GdNi_2$.

The MCE properties of $DyNi_2$, which orders at 21 K, have been studied by several authors (92, 93, 120). The ΔS_M value was reported to be -283 mJ/cm^3 K for a field change of $\Delta H = 7$ T (93), -252 mJ/cm^3 K for $\Delta H = 5$ T (120), and -212 mJ/cm^3 K for $\Delta H = 5$T (92). The value by Tomokiyo et al (120) is ~20% greater than the other two values reported (92, 93), taking into account the differences in the field changes. The MCE peak for $DyNi_2$ samples is different, somewhat

sharper for the Tomokiyo et al sample ($\delta_{FWHM} = 16$ K) compared with the von Ranke et al sample ($\delta_{FWHM} = 23$ K) (92), whereas the $RCP(S)$ for the former (4040 mJ/cm^3) is about 15% smaller than that for the von Ranke et al sample (4790 mJ/cm^3). These differences could easily be accounted for in the sample preparation because there are many intermediate phases in the Dy-Ni system, most of which melt incongruently, including $DyNi_2$, making it difficult to prepare single phase materials. von Ranke et al (92) also determined $\Delta T_{ad} = 8.2$ K, and calculated the MCE properties using crystalline electric field theory and found good agreement with the experimental data.

Tomokiyo et al (120) determined the MCE effect, ΔS_M, of $HoNi_2$ and $ErNi_2$ from magnetization measurements for $\Delta H = 1$, 3, and 5 T. For the 5 T field the ΔS_M values were -234 and -252 mJ/cm^3 K at the Curie temperatures of 19.5 and 8 K, respectively. These ΔS_M values are consistent with the value they reported for $DyNi_2$.

The adiabatic temperature rise at the Curie temperature of $(Gd_{0.1}Dy_{0.9})Ni_2$ (27 K) was 10.6 K for a 0 to 7.5 T field change, which is fairly good (96). It is about the same as that of $TbNi_2$ and lies about halfway between GdPd and $(Dy_{0.5}Er_{0.5})Al_2$.

Several lanthanide-nickel-aluminum ternary (RAlNi for R = Gd, Dy and Er) and quaternary [(Gd_xEr_{1-x})AlNi] alloys have been studied. The ternary compound DyAlNi was studied for its MCE properties. DyAlNi orders magnetically at 28 K and has a small $\Delta T_{ad} = 6.4$ K for a 0 to 7.5 T magnetic field change (96). Furthermore, its MCE peak appears to be quite broad, and ΔT_{ad} is nearly constant from 28 to ~35 K, with a slight temperature drop (~0.2 K) with increasing temperature. Above ~35 K the published results are probably not reliable.

Of the 10 (Gd_xEr_{1-x})AlNi alloys studied, only ErAlNi exhibits one ordering temperature (35, 121); others exhibit several (up to 4) magnetic transitions (35, 96, 121, 122). The multiple magnetic transitions give rise to broad-peaked magnetocaloric effects (both ΔT_{ad} and ΔS_M) for most alloys. The three exceptions are $(Gd_{0.20}Er_{0.80})$AlNi, $(Gd_{0.40}Er_{0.60})$AlNi, and $(Gd_{0.45}Er_{0.55})$AlNi, which exhibit broader caret-like peaks, approximately 50% broader than that for the ErAlNi compound for a 0 to 5 T field change. The ΔT_{ad} values are 6.3, 6.7, 6.1, and 5.5 K for $x = 0$, 0.20, 0.40 and 0.45, respectively, while the corresponding δT_{FWHM} values are 23, 34, 38, and 38 K, respectively (35, 121). For $(Gd_{0.20}Er_{0.80})$AlNi, $(Gd_{0.40}Er_{0.60})$AlNi, and $(Gd_{0.45}Er_{0.55})$AlNi, the magnetic ordering temperatures are similar enough that the MCE still has one peak and has not begun to flatten out to give rise to a table-like (96, 122) or skewed caret-like (35, 121) peak, as observed for alloys with $x \geq 0.5$, and a much broader δT_{FWHM} value (two to three times that of the ErAlNi compound). Although magnetocaloric ΔT_{ad} values for the Gd-rich (Gd_xEr_{1-x})AlNi phases are ~50% smaller than those of the RAl_2 phases, their flatness may be a distinct advantage for certain magnetic refrigeration cycles. For an Ericsson cycle one would like to have a constant ΔS_M value, which is found in $(Gd_{0.54}Er_{0.45})$AlNi from ~15 to ~45 K (122). Indeed, Takeya et al (122) showed that this alloy could be substituted for some complex multicomponent

multilayered (three or four) RAl_2 phases in an Ericsson hydrogen gas liquefier. Korte et al (35, 121) noted that the skewed caret-like magnetocaloric effect curves may actually be better active magnetic regenerator (AMR) materials than those substances with normal caret-like behaviors because the AMR thermodynamic cycle operates best as ΔT_{ad} rises at a rate of about 1 K per 1 K, which is better approximated by the skewed caret-like magnetocaloric peaks than the normal caret-like behavior which may rise at rates much higher than this, i.e. 2 or 3 K per 1 K.

Amorphous Alloys

Only few amorphous alloys have been studied with respect to their magnetocaloric effect. The major effort in studying the MCE of amorphous materials focused on various alloys containing lanthanide and transition metals, which were prepared by rapid solidification (melt spinning) of arc-melted alloy buttons (76, 123–127). This class of materials generally shows quite broad magnetic ordering transitions, which result in much lower $|\partial M/\partial T|$ at constant magnetic field, and therefore, the observed peak $\Delta S_M(T)_{\Delta H}$ and $\Delta T_{ad}(T)_{\Delta H}$ are considerably lower (Equations 4 and 9) than those of their crystalline alloy counterparts.

Most of the amorphous $R_{1-x}M_x$ alloys, where M = transition metal, display nearly a conventional MCE (both ΔS_M and ΔT_{ad}) behavior. Amorphous $Gd_{0.7}Fe_{0.3}$ has a peak of -10.2 mJ/cm^3 K at 286 K for $\Delta H = 1$ T (123). When Fe is partially substituted by Ni in $Gd_{0.7}Fe_{0.12}Ni_{0.18}$, the MCE peak temperature is reduced to 172 K, and the peak MCE value is -63 mJ/cm^3 K (-9.0 mJ/cm^3 K per T) for $\Delta H = 7$ T (123). Complete substitution of Fe by Co also causes the reduction in the peak MCE temperature in the amorphous $Gd_{0.65}Co_{0.35}$ alloy (124). The ΔS_M reaches only -30 mJ/cm^3 K (-3.8 mJ/cm^3 K per T), and the ΔT_{ad} reaches 2.8 K for $\Delta H = 8$ T as calculated from heat capacity data by Liu et al (124). The $Gd_{0.7}Ni_{0.3}$ alloy has maximum MCE at 124 K reaching -58 mJ/cm^3 K (-7.2 mJ/cm^3 K per T) and 3.3 K for $\Delta H = 8$ T as calculated from heat capacity (123, 124). The ΔS_M calculated from magnetization data is significantly higher, reaching -90 mJ/cm^3 K (-12.9 mJ/cm^3 K per T) for $\Delta H = 7$ T (125). When nonmagnetic Cu is introduced in amorphous Gd-based alloys, the MCE peak temperature is 141 K for $Gd_{0.7}Cu_{0.3}$, and ΔS_M peaks at -65 mJ/cm^3 K (-9.3 mJ/cm^3 K per T) for $\Delta H = 7$ T (123) and ΔT_{ad} at 3.6 K for $\Delta H = 8$ T (126).

Amorphous alloys containing Dy were studied for the following compositions: $Dy_{0.7}Fe_{0.3}$ (123, 124), $Dy_{0.7}Fe_{0.12}Ni_{0.18}$ (123, 125), $Dy_{0.7}Ni_{0.3}$ (123, 125), $Dy_{0.7}Cu_{0.3}$ (126), $Dy_{0.7}Zr_{0.3}$ (127), and $Dy_{0.3}Zr_{0.7}$ (127). Their peak MCE temperatures are considerably lower than those of the corresponding Gd alloys varying from 108 K ($Dy_{0.7}Fe_{0.3}$) to 48 K ($Dy_{0.7}Ni_{0.3}$). The maximum ΔS_M and ΔT_{ad} are slightly different from those observed in Gd-containing alloys, but the difference generally is within experimental error, indicating that the nature of lanthanide metal has almost no effect on the MCE of this class of amorphous alloys. As dilution of lanthanide metal increases ($Dy_{0.7}Zr_{0.3}$ versus $Dy_{0.3}Zr_{0.7}$), the shape of the MCE behavior becomes extremely broad, almost flat, with a very low ΔS_M (127).

When Er is substituted for Dy, a further reduction of the peak MCE temperature is observed: amorphous $Er_{0.7}Fe_{0.3}$ has ΔS_M of -106 mJ/cm^3 K (-13 mJ/cm^3 K per T) and a ΔT_{ad} of 3.6 K at $\sim$35 K for a magnetic field change of 8 T (124).

Only one amorphous alloy of different chemical nature has been studied (128); its composition is $Fe_{0.05}Co_{0.70}Si_{0.15}B_{0.0}$. The low magnetic field ($\Delta H = 1$ T) MCE measured directly also shows conventional behavior reaching 0.11 K at 645 K. At low temperatures, the MCE behavior becomes anomalous, showing a positive and then a negative deviation from smooth behavior as temperature increases from 390 to 465 K. This behavior was thought to be associated with temperature dependence of magnetic anisotropy constant (128).

Although the amount of experimental data characterizing various classes of amorphous magnetic alloys is not extensive, it is possible to predict that these materials could only be suitable as magnetic refrigerant materials at low temperatures ($<$20 K), where the lattice heat capacity is low. As noted above, this is associated with intrinsically low $|\partial M/\partial T|$, which translates to a low ΔT_{ad} away from absolute zero; thus these alloys are hardly suitable for practical magnetic refrigeration applications.

Manganites

The lanthanum-manganese perovskite compounds $(La_{1-x}M_x)MnO_3$, where M = Li, Na, K, Ca, Sr, Ba, and Y, have recently been heavily studied for the magnetocaloric properties since the discovery by Morelli et al (129) that several of these phases have reasonable, but not outstanding, magnetocaloric effect values (about one-third of Gd metal at best) in the temperature range from 250 to 350 K. Subsequently, others (130–139) have found that several of these phases have values comparable to that of gadolinium, $\Delta S_M = -23.7$ mJ/cm^3 K, for a 0 to 1 T field change (see Table 3). The lanthanum manganites with the highest magnetocaloric effect values are $(La_{1-x}Ca_x)MnO_3$ phases for $0.20 \leq x \leq 0.33$ with ΔS_M values ranging from -18.2 to -21.8 mJ/cm^3 K per T. It should be pointed out that Morelli et al (129) also measured the magnetocaloric effect for $La_{0.67}Ca_{0.33}MnO_3$; they found a much smaller ΔS_M value, ~ -4.8 mJ/cm^3 K (as estimated from the 1 and 2 T field changes), but a much wider breadth of the peak, $\delta T_{FWHM} = 62$ K, than what Guo et al (133) reported, $\Delta S_M = -32.7$ mJ/cm^3 K and $\delta T_{FWHM} = 11$ K for a field change of 1.5 T. This discrepancy needs to be examined. It could be due to differences in the sample preparation, or slight differences in composition. The ordering temperatures for these alkaline earth metal substitutes range from 225 to 260 K. Although their ΔS_M values may be comparable to Gd, they are significantly smaller than those observed in the $Gd_5(Si_xGe_{1-x})_4$ system, e.g. $\Delta S_M = -143$ mJ/cm^3 K for $Gd_5(Si_2Ge_2)$ ($T_C = 275$K) and -538 mJ/cm^3 K for $Gd_5(SiGe_3)$ ($T_C = 140$ K) for $\Delta H = 5$ T (see Table 1), which corresponds to -28 and -108 mJ/cm^3 K per T (40). The *RCP*(*S*) of $La_{0.67}Ca_{0.33}MnO_3$ for the two measurements is comparable and fairly large 208 (128) versus 240 mJ/cm^3 (133) per T and suggests that compositions near $x = 0.33$ ($La_{1-x}Ca_xMnO_3$) are potential magnetic refrigerant candidate materials, along with lower calcium concentration materials $0.2 \leq x \leq 0.3$.

TABLE 3 The magnetic ordering temperature and magnetocaloric properties of the lanthanum-manganese-based perovskite phases. Corresponding values for gadolinium metal are also included for a comparison basis

Composition	T_{max} (K)	$-\Delta S_M$ (mJ/cm^{3}K)	δT_{FWHM} (K)	$-RCP(S)$ (mJ/cm^3)	ΔH (T)	$-\Delta S_M/\Delta H$ (mJ/cm^{3}KT)	Reference
(La-Na)MnO_3							
$La_{0.925}Na_{0.075}MnO_3$	195	8.27	70	579	1	8.3	130
$La_{0.90}Na_{0.10}MnO_3$	218	9.44	60	566	1	9.4	130
$La_{0.898}Na_{0.072}Mn_{0.971}O_3$	193	7.75	69	535	1	7.8	131
$La_{0.880}Na_{0.999}Mn_{0.977}O_3$	220	8.99	57	512	1	9.0	131
$La_{0.835}Na_{0.165}MnO_3$	342	12.9	30	387	1	12.9	130
$La_{0.834}Na_{0.163}MnO_{2.99}$	343	12.9	30	387	1	12.9	131
$La_{0.80}Na_{0.20}MnO_3$	334	11.7	44	515	1	11.7	130
$La_{0.799}Na_{0.1.99}MnO_{2.97}$	334	12.0	45	540	1	12.0	131
(La-K)MnO_3							
$La_{0.893}K_{0.078}Mn_{0.965}O_3$	230	7.50	156	1170	1.5	5.0	132
$La_{0.877}K_{0.096}Mn_{0.974}O_3$	283	9.11	120	1090	1.5	6.1	132
$La_{0.813}K_{0.160}Mn_{0.987}O_3$	338	12.7	61	777	1.5	8.5	132
$La_{0.796}K_{0.196}Mn_{0.993}O_3$	334	13.1	54	710	1.5	8.7	132
(La-Ca)MnO_3							
$La_{0.8}Ca_{0.2}MnO_3$	230	32.7	13	425	1.5	21.8	133
$La_{0.75}Ca_{0.25}MnO_3$	225	27.4	21	575	1.5	18.2	134
$La_{0.67}Ca_{0.33}MnO_3$	252	12.2	85	1040	5	2.4	129
$La_{0.67}Ca_{0.33}MnO_3$	260	32.7	11	360	1.5	21.8	133
$La_{0.67}Ca_{0.33}MnO_3$	259	15.3	44	675	3	5.1	136
$La_{0.6}Ca_{0.4}MnO_3$	263	29.6	27	801	3	9.9	135
$La_{0.55}Ca_{0.45}MnO_3$	238	11.2	36	403	1.5	7.5	133

(*Continued*)

TABLE 3 (*Continued*)

Composition	T_{max} (K)	$-\Delta S_M$ (mJ/cm^{3}K)	δT_{FWHM} (K)	$-RCP(S)$ (mJ/cm^3)	ΔH (T)	$-\Delta S_M/\Delta H$ (mJ/cm^{3}KT)	Reference
(La-Sr)MnO_3							
$La_{0.75}Sr_{0.25}MnO_3$	340	8.7	43	374	1.5	5.8	137
$La_{0.7}Sr_{0.3}MnO_3$	312	13.3	–	–	6	2.2	138
$La_{0.67}Sr_{0.33}MnO_3$	348	9.97	125	1250	5	2.0	129
(La-Ba)MnO_3							
$La_{0.67}Ba_{0.33}MnO_3$	292	8.73	109	952	5	1.7	129
(La-Li)(Ti-Mn)O_3							
$La_{0.958}Li_{0.025}Ti_{0.1}Mn_{0.9}O_3$	90	12.0[a]	64	768	3	4.0	135
$La_{0.917}Li_{0.05}Ti_{0.2}Mn_{0.8}O_3$	77	10.2[a]	71	724	3	3.4	135
$La_{0.85}Li_{0.15}Ti_{0.3}Mn_{0.7}O_3$	60	6.60[a]	81	535	3	2.2	135
$La_{0.83}Li_{0.1}Ti_{0.4}Mn_{0.6}O_3$	35	5.40[a]	72	389	3	1.8	135
(La-Ca)(T i-Mn)O_3							
$La_{0.65}Ca_{0.35}Ti_{0.1}Mn_{0.9}O_3$	103	7.71[b]	140	1080	3	2.6	135
$La_{0.65}Ca_{0.35}Ti_{0.2}Mn_{0.8}O_3$	87	5.34[b]	137	732	3	1.8	135
$La_{0.65}Ca_{0.35}Ti_{0.4}Mn_{0.6}O_3$	42	3.56[b]	92	328	3	1.2	135
(La-Sr-Ca)MnO_3							
$La_{0.75}Sr_{0.175}Ca_{0.075}MnO_3$	330	16.6	25	415	1.5	11.1	137
$La_{0.75}Sr_{0.15}Ca_{0.1}MnO_3$	335	16.6	25	415	1.5	11.1	137
$La_{0.75}Sr_{0.125}Ca_{0.125}MnO_3$	282	8.71	72	627	1.5	5.8	137

(La-Y-Ca)MnO_3							
$La_{0.60}Y_{0.07}Ca_{0.33}MnO_3$	230	8.59	96	825	3	2.9	136
(La-Y-Sr)MnO_3							
$La_{0.65}Y_{0.05}Sr_{0.3}MnO_3$	320	29.6	52	1540	6	4.9	138
$La_{0.60}Y_{0.10}Sr_{0.3}MnO_3$	265	25.8	70	1810	6	4.3	138
$La_{0.55}Y_{0.15}Sr_{0.3}MnO_3$	215	21.1	77	1620	6	3.5	138
$La_{0.50}Y_{0.2}Sr_{0.3}mnO_3$	185	24.0	75	1800	6	4.0	138
(La-Ca)Mn_2O_7							
$La_{1.6}Ca_{1.4}Mn_2O_7$	168	21.0	42	882	1.5	14.0	139
Gd							
Gd	294	23.7	20	474	1	23.7	14[c]
Gd	294	33.1	30	993	1.5	22.1	14[c]
Gd	294	42.8	33	1410	2	21.4	14[c]
Gd	294	56.9	45	2560	3	18.0	14[c]
Gd	294	81.4	63	5120	5	16.3	14[c]
Gd	294	92.4	72	6650	6	15.4	14[c]

[a]Assumed density of 6.00g/cm^3

[b]Assumed density of 5.93g/cm^3

[c]Y Spichkin, unpublished data; Ames Laboratory

From the known magnetic/structural/electronic $(La_{1-x}Ca_x)MnO_3$ phase diagram (140), these compositions exhibit a ferromagnetic insulator/ferromagnetic metal transition for $0.18 \leq x \leq 0.28$, or a ferromagnetic metal/paramagnetic insulator transition for $0.28 \leq x \leq 0.50$, which probably accounts for their enhanced magnetocaloric properties. To date only one direct measurement of the adiabatic temperature change has been made (141). The ΔT_{ad} value of $La_{0.6}Ca_{0.4}MnO_3$ (2.1 K for a 3 T field change at $T_C = 260$ K) was calculated from heat capacity measurements and is about what one might expect for the composition of this material and its ΔS_M relative to the other perovskite phases. In view of the reported ΔS_M values and the ability to adjust the magnetic ordering temperature from 40 to 350 K (see Table 3) by varying the La to M ratio and the chemical nature of M, a great deal of fundamental and applied research can be expected in the next few years on these materials.

EPILOGUE

Research in the last few years on the magnetocaloric effect has led to several exciting discoveries and has advanced the technical aspects of magnetic refrigeration such that it appears that magnetic cooling and refrigeration may be competitive with the common vapor cycle gas compression technology.

Several new magnetocaloric substances with substantial cooling capacity have been discovered: (*a*) the lanthanide aluminides $(Dy_xEr_{1-x})Al_2$ for the 10–70 K range; (*b*) the (R,R′)AlNi phases (R and R′ different lanthanide metals), which have multiple magnetic transitions and thus unusual MCE temperature dependences in the 5 to 65 K range; (*c*) the La manganites, some of which have MCEs comparable to Gd between 220 and 290 K; and (*d*) the tunable giant MCE $Gd_5(Si_xGe_{1-x})_4$ materials for the unheard of 40 to 290 K temperature span. The latter two along with the well established Gd and Gd-R alloys offer considerable promise that practical near room–temperature magnetic refrigeration/cooling is just around the corner.

Indeed, technical advances (though just briefly discussed in this review) toward a commercial reality for air conditioning and refrigerater/freezers, have generated much interest in understanding the fundamental aspects of electronic and magnetic phenomena, especially as related to the magnetocaloric effect. One important aspect is the role that first order magnetic transitions may have on the giant MCE, especially since such a transformation may exhibit strong hysteresis and kinetic effects. Although complete answers do not exist today, they will surely blossom forth in the not-too-distant future.

ACKNOWLEDGMENTS

The authors thank their colleagues Jessica Anderson, Jake Auliff, and Paul Tomlinson for assistance in compiling the numerical data used in this review;

Alexandra Pecharsky and Youri Spichkin for allowing us to use some of their unpublished results; and Alexander Tishin (Moscow State University) for supplying copies of some papers that were unavailable to the authors. This work was partially supported by both the Materials Science Division, Office of Basic Energy Sciences and the Laboratory Technology Research Program, Office of Computational and Technology Research, both of the U.S. Department of Energy. The Ames Laboratory is operated by Iowa State University for the U.S. Departmet of Energy under contract no. W-7405-ENG-82.

NOTE ADDED IN PROOF

After this manuscript was completed, an excellent review by Tishin (142) describing various aspects of magnetocaloric effect and magnetic refrigeration appeared in the literature.

LITERATURE CITED

1. Warburg E. 1881. *Ann. Phys. (Leipzig)* 13:141–64
2. Debye P. 1926. *Ann. Phys.* 81:1154–60
3. Giauque WF. 1927. *J. Am. Chem. Soc.* 49:1864–70
4. Giauque WF, MacDougall DP. 1933. *Phys. Rev.* 43:768
5. Collins SC, Zimmerman FJ. 1953. *Phys. Rev.* 90:991–92
6. Heer CV, Barnes CB, Daunt JC. 1954. *Rev. Sci. Instr.* 25:1088–98
7. Brown GV. 1976. *J. Appl. Phys.* 47:3673–80
8. Steyert WA. 1978. *J. Appl. Phys.* 49:1216–26
9. Barclay JA, Steyert WA. 1982. *U.S. Patent No. 4332135*
10. Barclay JA. 1983. *U.S. Patent No. 4408463*
11. Kirol LD, Dacus M. 1988. *Adv. Cryog. Eng.* 33:757–65
12. Al'tov VA, Brodyanskii VM, Karagusov VI, Kurguzov VV, Sunyavskii YV, Sychev VV. 1988. *Sov. Phys. Dokl.* 33:759–61
13. Green G, Shafe J. 1990. *Adv. Cryog. Eng.* 35B:1165–74
14. DeGregoria AJ, Barclay JA, Claybaker PJ, Jaeger SR, Kral ZF, et al. 1990. *Adv. Cryog. Eng.* 35:1125–31
15. DeGregoria AJ, Feuling LJ, Lattsch JF, Rowe JR, Trueblood JR, Wang AA. 1992. *Adv. Cryog. Eng.* 37B:875–82
16. Janda D, DeGregoria T, Johnson J, Kral S, Kinrad G. 1992. *Adv. Cryog. Eng.* 37B:891–98
17. Filin NV, Mikhailov II, Dovbish AL, Ronjin PL. 1992. *IEEE Trans. Magn.* 28:953–56
18. Zimm CB, Johnson JW, Murphy RW. 1996. *Adv. Cryog. Eng.* 41B:1675–81
19. Nellis GF, Smith JL Jr. 1996. *Adv. Cryog. Eng.* 41B:1665–73
20. Numazawa T. 1997. *Teion Kogaku* 32: 192–202
21. Zimm CB, DeGregoria AJ. 1992. *Proc. 6th Intern. Conf. Superconduct. Applications, Buffalo, NY*, pp. 471–80. AIP Conf. Proc. No. 273. College Park, MD: Am. Inst. Phys.
22. Zimm C, Jastrab A, Sternberg A, Pecharsky V, Gschneidner K Jr, et al. 1998. *Adv. Cryog. Eng.* 43:1759–66

23. Morrish AH. 1965. *The Physical Principles of Magnetism*, pp. 78–83. New York: Wiley & Sons. 680 pp.
24. Tishin AM, Gschneidner KA Jr, Pecharsky VK. 1999. *Phys. Rev. B* 59:503–11
25. Dan'kov SY, Tishin AM, Pecharsky VK, Gschneidner KA Jr. 1998. *Phys. Rev. B* 57:3478–90
26. Pecharsky VK, Gschneidner KA Jr. 1996. *Adv. Cryog. Eng.* 42:423–30
27. Gschneidner KA Jr, Pecharsky VK. 1997. In *Rare Earths: Science, Technology and Applications III*, ed. RG Bautista, CO Bounds, TW Ellis, BT Kilbourn, pp. 209–22. Warrendale, PA: Miner. Met. Mater. Soc.
28. Benford SM, Brown GV. 1981. *J. Appl. Phys.* 52:2110–12
29. Tishin AM. 1990. *Cryogenics* 30:127–36
30. Dan'kov SY, Tishin AM, Pecharsky VK, Gschneidner KA Jr. 1997. *Rev. Sci. Inst.* 68:2432–37
31. Hashimoto T, Numusawa T, Shino M, Okada T. 1981. *Cryogenics* 21:647–53
32. Ponomarev BK. 1986. *J. Magn. Magn. Mater.* 61:129–38
33. Gopal BR, Chahine R, Bose TK. 1997. *Rev. Sci. Instr.* 68:1818–22
34. Giguere A, Földeaki M, Gopal RB, Chahine R, Bose TK, et al. 1999. *Phys. Rev. Lett.* 83:2262–65
35. Korte BJ, Pecharsky VK, Gschneidner KA Jr. 1998. *J. Appl. Phys.* 84:5677–85
36. Gschneidner KA Jr, Takeya H, Moorman JO, Pecharsky VK. 1994. *Appl. Phys. Lett.* 64:253–55
37. Gschneidner KA Jr, Pecharsky VK, Malik SK. 1996. *Adv. Cryog. Eng.* 42A:475–82
38. McEven KA. 1978. In *Handbook on the Physics and Chemistry of Rare Earths*, ed. KA Gschneidner Jr, LR Eyring, 1:411– 88. Amsterdam: North-Holland
39. Pecharsky VK, Gschneidner KA Jr. 1997. *Phys. Rev. Lett.* 78:4494–97
40. Pecharsky VK, Gschneidner KA Jr. 1997. *Appl. Phys. Lett.* 70:3299–301
41. Pecharsky VK, Gschneidner KA Jr. 1997. *J. Magn. Magn. Mater.* 167:L179–84
42. Pecharsky VK, Gschneidner KA Jr. 1998. *Adv. Cryog. Eng.* 43:1729–36
43. Nikitin SA, Myalikgulev G, Tishin AM, Annaorazov MP, Asatryan KA, Tyurin AL. 1990. *Phys. Lett. A* 148:363–66
44. Annaorazov MP, Asatryan KA, Myalikgulyev G, Nikitin SA, Tishin AM, Tyurin AL. 1992. *Cryogenics* 32:867–72
45. Annaorazov MP, Nikitin SA, Tyurin AL, Asatryan KA, Dovletov AK. 1996. *J. Appl. Phys.* 79:1689–95
46. Belova VM, Nikolaev VI, Stuchebnikov VM. 1974. *Prib. Tekh. Eksp.* 1:209–11
47. Ponomarev BK. 1983. *Prib. Tekh. Eksp.* 3:153–55
48. Green G, Chafe J, Stevens J, Humphrey J. 1990. *Adv. Cryog. Eng.* 35B:1165–74
49. Kato H, Nara K, Okaji M. 1991. *Cryogenics* 31:425–30
50. Otowski W, Glorieux C, Hofman R, Thoen J. 1993. *Thermochim. Acta* 218: 123–33
51. Gopal BR, Chahine R, Földeaki M, Bose TK. 1995. *Rev. Sci. Instrum.* 66:232–38
52. Levitin RZ, Snegirev VV, Kopylov AV, Lagutin AS, Gerber A. 1997. *J. Magn. Magn. Mater.* 170:223–27
53. Földeaki M, Chahine R, Bose TK. 1995. *J. Appl. Phys.* 77:3528–37
54. Pecharsky VK, Gschneidner KA Jr. 1999. *J. Appl. Phys.* 86:565–75
55. Pecharsky VK, Gschneidner KA Jr. 1999. *J. Appl. Phys.* 86:6315–21
56. Zimm CB, Ratzmann PM, Barclay JA, Green GF, Chafe JN. 1990. *Adv. Cryog. Eng.* 36:763–68
57. Nikitin SA, Talalaeva EV, Chernikova LA, Chuprikov GE, Ivanova TI, et al. 1978. *Zh. Eksp. Teor. Fiz.* 74:205–13; *Sov. Phys. JETP* 47:105–9 (Eng. Transl.)
58. Ivanova TI, Levitin RZ, Nikitin SA, Talalaeva EV, Chernikova LA. 1981. *Fiz. Met. Metalloved.* 51:893–96; *Phys. Met. Metall.* 51(4):196–99 (Eng. Transl.)

59. Tishin AM. 1990. *Pis'ma Zh. Tekh. Fiz.* 16:12–16; *Sov. Tech. Phys. Lett.* 16:47–49 (Eng. Transl.)
60. Dan'kov SY, Spichkin YI, Tishin AM. 1996. *J. Magn. Magn. Mater.* 152:208–12
61. Glorieux C, Caerels J, Thoen J. 1996. *J. Appl. Phys.* 80:3412–21
62. Nikitin SA, Andreyenko AS, Tishin AM, Arkharov AM, Zherdev AA. 1985. *Fiz. Metal. Metalloved.* 60:689–94; *Phys. Met. Metall.* 60(4):56–61 (Eng. Transl.)
63. Green G, Patton W, Stevens J. 1988. *Adv. Cryog. Eng.* 33:777–83
64. Nikitin SA, Tishin AM, Bykhova SE. 1989. *Phys. Stat. Solidi A* 114:K99–101
65. Chen GL, Mei VC, Chen FC. 1992. *J. Appl. Phys.* 72:3908–11
66. Kuz'min MD, Tishin AM. 1993. *Cryogenics* 33:868–82
67. Hudgins AC, Pavlovic AS. 1965. *J. Appl. Phys.* 36:3628–31
68. Benford SM. 1979. *J. Appl. Phys.* 50: 1868–70
69. Nikitin SA, Tishin AM, Leontiev PI. 1991. *J. Magn. Magn. Mater.* 92:405–16
70. Nikitin SA, Andreyenko AS, Tishin AM, Arkharov AM, Zherdev AA. 1985. *Fiz. Metal. Metalloved.* 59:327–31; *Phys. Met. Metall.* 59:104–7 (Eng. Transl.)
71. Zimm CB, Kral PL, Barclay JA, Green GF, Patton WG. 1988. *Proc. 5th Intern. Cryocooler Conf. Monterey, CA.* pp. 49–57. Wright-Patterson Air Force Base, OH: Wright Research and Development Center
72. Zimm CB, Barclay JA, Harkness HH, Green GF, Patton WG. 1989. *Cryogenics* 29:937–38
73. Coey JMD, Skumaryev V, Gallagher K. 1999. *Nature* 401:35–36
74. Shao YZ, Lai JKL, Shek CH. 1996. *J. Magn. Magn. Mater.* 163:103–8
75. Shao Y, Zhang J, Lai JKL, Shek CH. 1996. *J. Appl. Phys.* 80:76–80
76. Földeaki M, Chahine R, Gopal BR, Bose TK, Liu XY, Barclay JA. 1998. *J. Appl. Phys.* 83:2727–34
77. Földeaki M, Schnelle W, Gmelin E, Benard P, Koszegi B, et al. 1997. *J. Appl. Phys.* 82:309–16
78. Nikitin SA, Tishin AM, Red'ko SV. 1988. *Fiz. Metal. Metalloved.* 66:86–94; *Phys. Met. Metall.* 66:77–85 (Eng. Transl.)
79. Smaili A, Chahine R. 1997. *J. Appl. Phys.* 81:824–29
80. Burkhanov GS, Dan'kov, SY, Nikitin SA, Tishin AM, Chistyakov OD. 1991. *Pis'ma Zh. Tekh. Fiz.* 17:7–11; *Sov. Tech. Phys. Lett.* 17:353–55 (Eng. Transl.)
81. Tishin AM. 1990. *Cryogenics* 30:720–25
82. Smaïli A, Chahine R. 1996. *Adv. Cryog. Eng.* 42:445–50
83. Nikitin SA, Tishin AM. 1989. *Fiz. Metal. Metalloved.* 67:273–78; *Phys. Met. Metall.* 67(2):59–64 (Eng. Transl.)
84. Nikitin SA, Andreyenko AS. 1981. *Fiz. Met. Metalloved.* 52:67–71; *Phys. Met. Metall.* 52(1):55–59 (Eng. Transl.)
85. Nikitin SA, Andreyenko AS, Chuprikov GE, Posyado VP. 1977. *Zh. Eksp. Teor. Fiz.* 73:728–36; *Sov. Phys. JETP* 46:118–22 (Eng. Transl.)
86. Nikitin SA, Tishin AM, Leontev PI. 1989. *Phys. Stat. Solidi A.* 113:K117–21
87. Zimm CB. 1994. *Adv. Cryog. Eng.* 40: 647–53
88. Pecharsky, VK, Gschneidner KA Jr, Dan'kov SYu, Tishin AM. 1999. *In Cryocoolers 10,* ed. RG Ross Jr, pp. 639–45. New York: Kluwer/Plenum
89. Pecharsky VK, Gschneidner KA Jr, Zimm CB. 1996. *Adv. Cryog. Eng.* 42: 451–58
90. Hashimoto T, Matsumoto K, Kurihara T, Numazawa T, Tomokiyo A, et al. 1986. *Adv. Cryog. Eng.* 32:279–86
91. Gschneidner KA Jr, Pecharsky VK, Gailloux MJ, Takeya H. 1996. *Adv. Cryog. Eng.* 42:465–74
92. von Ranke PJ, Pecharsky VK, Gschneidner KA Jr. 1998. *Phys. Rev. B.* 58:12110–16
93. Földeaki M, Giguere A, Chahine R, Bose TK. 1998. *Adv. Cryog. Eng.* 43:1533–40

94. Daudin B, Bonjour E. 1982. *Compt. Rend. Acad. Sci. Paris* 295:535–38
95. Zimm CB, Ludeman EM, Severson MC, Henning TA. 1992. *Adv. Cryog. Eng.* 37B:883–90
96. Gschneidner KA Jr, Takeya H, Moorman JO, Pecharsky VK, Malik SK, Zimm CB. 1994. *Adv. Cryog. Eng.* 39:1457–65
97. Barclay JA, Overton WC Jr, Zimm CB. 1984. In *Proc. 17th Int. Conf. Low Temperature Physics.* ed. U Eckern, A Schmid, H Wühl, pp. 157–58. Amsterdam: Elsevier
98. Pecharsky VK, Gschneidner KA Jr. 1997. *J. Alloys Compd.* 260:98–106
99. Gschneidner KA Jr, Pecharsky VK, Pecharsky AO, Zimm CB. 1999. *Mater. Sci. Forum* 315–317:69–76
100. Choe W, Pecharsky VK, Miller GJ, Pecharsky AO, Gschneidner KA Jr, Young VA. 2000. *Phys. Rev. Lett.* 84:
101. Hashimoto T. 1986. *Adv. Cryog. Eng.* 32:261–70
102. Pecharsky VK, Gschneidner KA Jr. 1999. In *Cryocoolers 10.* ed. RH Ross Jr, pp. 629–37. New York: Kluwer/Plenum
103. Potter HH. 1934. *Proc. R. Soc. London Ser. A* 146:362–87
104. Hirschler W, Rocker W. 1966. *Z. angew. Phys.* 21:368–72
105. Rocker W, Kohlhaus R. 1967. *Z. angew. Phys.* 23:146–54
106. Weiss P, Piccard A. 1918. *Compt. Rend.* 166:352–54
107. Weiss P, Forrer R. 1924. *Compt. Rend.* 178:1347–51
107a. Weiss P, Forrer R. 1926. *Ann. Phys.* 5:153–213
108. Noakes JE, Arrott AS. 1973. *18th Ann. Conf. Magn. Magn. Mater. Denver, CO 1972*, Part 2, pp. 899–903. New York: Am. Inst. Phys.
109. Kittel C. 1966. *Introduction to Solid State Physics*, p. 461. New York: Wiley. 3rd ed.
110. Znamenskii BV, Fakidov IG. 1962. *Fiz. Metal. Metalloved.* 13:312–14; *Phys. Met. Metall.* 13(2):146–48 (Eng. Transl.)
111. Kuhrt Ch, Schittny Th, Bärner K. 1985. *Phys. Stat. Solidi A* 91:105–13
112. Maeda H, Sato M, Uehara M. 1983. *J. Jpn. Inst. Metal.* 47:688–91
113. Herbst JF, Fuerst CD, McMichael RD. 1996. *J. Appl. Phys.* 79:5998–6000
114. Tishin AM. 1994. *J. Adv. Mater.* 1:403–15
115. Nikitin SA, Talalaeva EV, Chernikova LA, Andreenko AS. 1973. *Zh. Eksp. Teor. Fiz.* 65:2058–62; *Sov. Phys. JETP* 38:1028–30 (Eng. Transl.)
116. Nikitin SA, Talalayeva YeV, Chernikova LA, Andreyenko AS. 1975. *Fiz. Metal. Metalloved.* 40:967–71; *Phys. Met. Metall.* 40(5):55–59 (Eng. Transl.)
117. Nikitin SA, Tishin AM. 1991. *Cryogenics* 31:166–67
118. Giguere A, Földeaki M, Schnelle W, Gmelin E. 1999. *J. Phys. Condens. Matter.* 11:6969–81
119. Tokai Y, Takahashi A, Sahashi M, Hashimoto T, Yayama H, Tomokiyo A. 1992. *Jpn. J. Appl. Phys.* 31:3332–35
120. Tomokiyo A, Yayama H, Wakabayashi H, Kuzuhara T, Hashimoto T, et al 1986. *Adv. Cryog. Eng.* 32:295–301
121. Korte BJ, Pecharsky VK, Gschneidner KA Jr. 1998. *Adv. Cryog. Eng.* 43:1737–44
122. Takeya H, Pecharsky VK, Gschneidner KA Jr, Moorman JO. 1994. *Appl. Phys. Lett.* 64:2739–41
123. Földeaki M, Giguere A, Gopal BR, Chahine R, Bose TK, et al. 1997. *J. Magn. Magn. Mater.* 174:295–308
124. Liu XY, Barclay JA, Gopal BR, Földeaki M, Chahine R, et al. 1996. *J. Appl. Phys.* 79:1630–41
125. Liu XY, Barclay JA, Földeaki M, Gopal BR, Chahine R, Bose TK. 1996. *Adv. Cryog. Eng.* 42:431–38
126. Liu XY, Barclay JA, Gopal BR, Földeaki M, Chahine R, Bose TK. 1997. *Proc. 16th Intern. Cryogenic Eng. Conf./Intern.*

Cryogenic Mater. Conf., ed. T Haruyama, T Mitsui, K Yamafuji, pp. 2065–68. Oxford, UK: Elsevier
127. Giguere A, Földeaki M, Dunlap RA, Chahine R. 1999. *Phys. Rev. B* 59:431–35
128. Belova VM, Stolyarov VL. 1984. *Fiz. Tverd. Tela* 26:851–53; *Sov. Phys. Solid State* 26:515–16 (Eng. Transl.)
129. Morelli DT, Mance AM, Mantese JV, Micheli AL. 1996. *J. Appl. Phys.* 79:373–75
130. Zhong W, Chen W, Ding WP, Zhang N, Du YW, Yan QJ. 1998. *Solid State Comm.* 106:55–58
131. Zhong W, Chen W, Ding WP, Zhang N, Hu A, et al. 1998. *Eur. Phys. J. B* 3:169–74
132. Zhong W, Chen W, Ding WP, Zhang N, Hu A, et al. 1999. *J. Magn. Magn. Mater.* 195:112–18
133. Guo ZB, Du YW, Zhu JS, Huang H, Ding WP, Feng D. 1997. *Phys. Rev. Lett.* 78:1142–45
134. Guo ZB, Zhang JR, Huang H, Ding WP, Du YW. 1997. *Appl. Phys. Lett.* 70:904–5
135. Bohigas X, Tejada J, del Barco E, Zhang XX, Sales M. 1998. *Appl. Phys. Lett.* 73:390–92
136. Zhang XX, Tejada J, Xin X, Sun GF, Wong KW, Bohigas X. 1996. *Appl. Phys. Lett.* 69:3596–98
137. Guo ZB, Yang W, Shen YT, Du YW. 1998. *Solid State Commun.* 105:89–92
138. Bose TK, Chahine R, Gopal BR, Foldeaki M, Barman A, et al. 1998. *Cryogenics* 38:849–51
139. Zhou TJ, Yu Z, Zhong W, Xu XN, Zhang HH, Du YW. 1999. *J. Appl. Physics* 85:7975–77
140. Coey JMD, Viret M, van Molnar S. 1999. *Adv. Phys.* 48:167–293
141. Bohigas X, Tejada J, Marinez-Sarrion ML, Tripp S, Black R. 2000. *J. Magn. Magn. Mater.* 208:85–92
142. Tishin AM. 1999. In *Handbook of Magnetic Materials*, ed. KHJ Buschow, 12:395–524. Amsterdam: Elsevier.

Annual Review of Materials Science
Volume 30, 2000

CONTENTS